NASA Technical Paper 1435

Similitude Requirements and Scaling Relationships as Applied to Model Testing

Chester H. Wolowicz, James S. Bowman, Jr.,
and William P. Gilbert

AUGUST 1979

NASA

NASA Technical Paper 1435

Similitude Requirements and Scaling Relationships as Applied to Model Testing

Chester H. Wolowicz,
Dryden Flight Research Center
Edwards, California
James S. Bowman, Jr., and William P. Gilbert
Langley Research Center
Hampton, Virginia

National Aeronautics
and Space Administration

Scientific and Technical
Information Branch

1979

SIMILITUDE REQUIREMENTS AND SCALING RELATIONSHIPS AS APPLIED TO MODEL TESTING

Chester H. Wolowicz
Dryden Flight Research Center

and

James S. Bowman, Jr. and William P. Gilbert
Langley Research Center

INTRODUCTION

Experimental data for scale-model aircraft are used to define the aerodynamic characteristics of full-scale aircraft, verify theoretically predicted aerodynamic characteristics, and provide data where theory is deficient. To apply the data to a full-scale aircraft or its components with maximum validity, certain similitude conditions must be met. The similitude of the geometric configurations is a fundamental requirement, as is the similitude of the angles of attack. Reynolds number and Froude number, as well as Mach number in the case of compressible flow conditions, are pertinent parameters for steady-state (static) or dynamic test conditions. A number of other similitude parameters may be important, depending on the test objectives and aircraft elasticity.

In general, any one experimental technique will not satisfy all the similitude requirements for correlation of wind-tunnel data with free-flight data or for correlation of free-flight data obtained from models of different scale. Most tests are designed for certain similitude conditions at the expense of other parameters. For example, an elastic, rigidly mounted wind-tunnel model tested at full-scale Mach number and dynamic pressure through an angle of attack range does not properly account for the effects of mass on elastic deformation except at one angle of attack at a steady level-flight condition. Inertial aerolastic effects that occur in maneuvering flight must be accounted for theoretically. A comparison of the aerodynamic characteristics of one free-flying model with those of a model of different scale or a full-scale aircraft at the same Mach number may not be

appropriate if Froude number similitude requirements are not met. A difference in Froude number could result in dissimilar angles of attack.

Although there are many references of limited scope in the literature on similitude, a comprehensive report is needed to clarify and summarize the many techniques for wind-tunnel and free-flight model testing with regard to similitude requirements, test objectives, and comparison of model and full-scale results. The fulfillment of this need is particularly appropriate in that remotely controlled, subscale, powered and unpowered models of advanced aircraft are currently being used to investigate stability, control, and handling qualities at routine as well as high-risk flight conditions. One of the prime factors necessary to determine the limitations of data obtained from a model is the degree to which the similitude requirements have been met.

This report provides a comprehensive review of the similitude requirements for the most general test conditions, from low-speed incompressible flow conditions to high-speed supersonic conditions. The fluid is considered to be a continuum that obeys the perfect gas laws for a fixed value of the adiabatic gas constant. The similitude requirements are considered in relation to the scaling requirements, test technique, test conditions, and test objectives. Limitations in test techniques are indicated, with emphasis on the free-flying model.

Scaling procedures are illustrated for free-flying models in incompressible and compressible flow. For incompressible flow, the kinematic properties are preserved by using velocities scaled from Froude number similitude requirements (Froude scaling). For compressible flow, the compressibility effects are preserved by using velocities scaled from Mach number similitude requirements (Mach scaling). In addition, summary tables and nomographs are presented to facilitate a rapid assessment of the scaling requirements for free-flying models and of the extent to which the requirements are satisfied for both Froude and Mach number similitude.

Although this report covers parameters encountered in dynamic model tests, it does not include discussions of other similarity effects that may be important in individual cases, such as the scaling of a viscous damper in the control system of a model with free control surfaces or, a more remote example, the scaling of physical parameters for an icing test. To prepare for such situations, the experimenter should refer to books on dimensional analysis, such as references 1 and 2.

SYMBOLS

Physical quantities in this report are given in the International System of Units (SI) and U.S. Customary Units. Details concerning the use of SI are given in reference 3.

a	generalized linear acceleration, m/sec^2 (ft/sec^2)
$\bar{a}_n$	normal load factor, g
b	wingspan, m (ft)
C_D, C_L, C_Y	aerodynamic drag, lift, and side-force coefficients, respectively
$(C_D)_n$	crossflow drag coefficient
$C_{L_{max}}$	maximum lift coefficient
C_{L_q}	$= \dfrac{\partial C_L}{\partial (q\bar{c}/2V)}$
C_{L_u}	$= V\dfrac{\partial C_L}{\partial u}$
C_{L_α}	$= \dfrac{\partial C_L}{\partial \alpha}$
$C_{L_{\dot{\alpha}}}$	$= \dfrac{\partial C_L}{\partial (\dot{\alpha}\bar{c}/2V)}$
$C_{L_{\delta_e}}$	$= \dfrac{\partial C_L}{\partial \delta_e}$
$C_{L_{\dot{\delta}_e}}$	$= \dfrac{\partial C_L}{\partial (\dot{\delta}_e\bar{c}/2V)}$
C_l, C_m, C_n	aerodynamic rolling moment, pitching moment, and yawing moment coefficients, respectively
C_{l_r}	$= \dfrac{\partial C_l}{\partial (rb/2V)}$
C_{l_β}	$= \dfrac{\partial C_l}{\partial \beta}$

$C_{l_{\dot{\beta}}}$ $= \dfrac{\partial C_l}{\partial (\dot{\beta} b/2V)}$

C_{m_q} $= \dfrac{\partial C_m}{\partial (q\bar{c}/2V)}$

C_{m_u} $= V\dfrac{\partial C_m}{\partial u}$

C_{m_α} $= \dfrac{\partial C_m}{\partial \alpha}$

$C_{m_{\dot{\alpha}}}$ $= \dfrac{\partial C_m}{\partial (\dot{\alpha}\bar{c}/2V)}$

$C_{m_{\delta_e}}$ $= \dfrac{\partial C_m}{\partial \delta_e}$

$C_{m_{\dot{\delta}_e}}$ $= \dfrac{\partial C_m}{\partial (\dot{\delta}_e \bar{c}/2V)}$

C_{m_0} zero-lift pitching moment coefficient

C_{n_r} $= \dfrac{\partial C_n}{\partial (rb/2V)}$

$C_{n_{\dot{r}}}$ $= \dfrac{\partial C_n}{\partial (\dot{r} b^2/4V^2)}$

C_{n_β} $= \dfrac{\partial C_n}{\partial \beta}$

$C_{n_{\dot{\beta}}}$ $= \dfrac{\partial C_n}{\partial (\dot{\beta} b/2V)}$,

c_l, c_m airfoil section lift and pitching moment coefficients, respectively (fig. 2)

$\bar{c}$	mean aerodynamic chord, m (ft)
E	tensile and compressive modulus of elasticity, N/cm^2 (lb/in^2)
EI'	bending stiffness, $N\text{-}cm^2$ ($lb\text{-}in^2$)
F	force, N (lb)
G	shear modulus of elasticity, N/cm^2 (lb/in^2)
GJ'	torsional stiffness, $N\text{-}cm^2$ ($lb\text{-}in^2$)
g	acceleration of gravity, m/sec^2 (ft/sec^2)
I	mass moment of inertia, $kg\text{-}m^2$ ($slug\text{-}ft^2$)
I'	second bending moment of area, cm^4 (in^4)
I_Y	mass moment of inertia about pitch axis, $kg\text{-}m^2$ ($slug\text{-}ft^2$)
J'	second torsional moment of area, cm^4 (in^4)
k	radius of gyration, m (ft)
l	characteristic dimension, m (ft)
M	Mach number
M'	moment, m-N (ft-lb)
M_n	crossflow Mach number (figs. 3 and 4)
m	mass, kg (slugs)
N_{Fr}	Froude number, $\frac{V^2}{lg}$
N_{fu}	number of fundamental units in dimensional analysis
N_{pq}	number of physical quantities considered in dimensional analysis
N_{Re}	Reynolds number, $\frac{\rho_f V l}{\mu} = \frac{V l}{\nu}$

$(N_{Re})_n$	crossflow Reynolds number (fig. 3)
N_{Str}	Strouhal number, $\frac{\omega l}{V}$
n	scale of model
p, q, r	roll, pitch, and yaw rates, respectively, rad/sec
p_f	fluid pressure, N/m^2 (lb/ft^2)
$\dot{q}$	pitch acceleration, rad/sec^2
$\bar{q}$	dynamic pressure, $1/2\rho_f V^2$, N/m^2 (lb/ft^2)
$\bar{q}_c$	stagnation pressure in compressible flow (eq. (9)), N/m^2 (lb/ft^2)
R	spin or turn radius, m (ft)
R_{V_s}	velocity of sound ratio, V_{s_m}/V_{s_A}
S	wing area, m^2 (ft^2)
T, T_0	free-stream and stagnation temperatures, respectively, K (°R)
t	time, sec
u	linear velocity along the x-axis, m/sec (ft/sec)
$\dot{u}$	linear acceleration along the x-axis, m/sec^2 (ft/sec^2)
V	velocity, m/sec (ft/sec)
V_s	velocity of sound, m/sec (ft/sec)
$\bar{v}$	specific volume, m^3/kg ($ft^3/slug$)
W	weight, N (lb)
$\ddot{z}$	normal linear acceleration, m/sec^2 (ft/sec^2)
α	angle of attack, deg or rad

$\dot{\alpha}$	rate of change of angle of attack, rad/sec
α'	generalized aerodynamic attitude, deg or rad
β	angle of sideslip, deg or rad
$\dot{\beta}$	rate of change of angle of sideslip, rad/sec
γ	adiabatic constant
γ'	helix angle, rad
δ	control surface position, deg or rad
δ_a, δ_e, δ_r	aileron, elevator, and rudder positions, respectively, deg or rad
$\dot{\delta}_a$, $\dot{\delta}_e$, $\dot{\delta}_r$	rate of change of aileron, elevator, and rudder positions, respectively, deg/sec or rad/sec
μ	absolute viscosity, $N \cdot sec/m^2$ ($lb \cdot sec/ft^2$)
ν	kinematic viscosity, μ/ρ_f, m^2/sec (ft^2/sec)
ρ_f	mass density of fluid, kg/m^3 ($slugs/ft^3$)
τ	reduced-time parameter, tV/l
φ	bank angle, deg or rad
φ'	generalized angular displacement, deg or rad
φ'_0	amplitude of oscillatory motion, deg
ψ_0	oscillatory amplitude in yaw, deg (fig. 5)
Ω	generalized angular rate, rad/sec
$\dot{\Omega}$	generalized angular acceleration, rad/sec^2
ω	frequency of oscillation, rad/sec

Superscripts:

a', b', c', ...	exponents used in dimensional analysis (appendix)

Subscripts:

A	airplane
m	model

SIMILITUDE REQUIREMENTS FOR FORCES AND MOMENTS

For similitude of the nondimensionalized aerodynamic characteristics and kinematics of a model relative to a full-size aircraft, the dependence of one physical quantity on others involved in the experiment must be the same for the model and the full-scale airplane. If the number of physical quantities associated with a stipulated phenomenon are N_{pq} in number, and if these quantities can be expressed in terms of no more than N_{fu} fundamental units, the general physical relationship between the phenomenon and the physical quantities can be expressed in the form of $N_{pq} - N_{fu}$ independent dimensionless parameters using dimensional analysis.

Although dimensional analysis requires that certain conditions (dimensionless parameters) be fulfilled in the model test for similitude, the completeness of the conditions to be fulfilled is dependent on the completeness of the number and kinds of physical quantities taken into consideration. In addition, once the dimensionless parameters are determined, it is necessary to ascertain which individual parameters will have important effects under various conditions.

In this section, consideration is given to the general similitude requirements for model tests. These requirements are derived from the functional dependence of the forces and moments on the geometry, kinematics, and aerodynamics of the aircraft. The forces and moments on an aircraft due to the motion of the aircraft through the fluid depend on the properties of the aircraft and the fluid, as well as the linear and angular velocities and accelerations, and displacement.

The pertinent properties of the fluid are its mass density, ρ_f; absolute viscosity, μ; and elasticity as defined by its velocity of sound, V_s. The pertinent properties of the aircraft include its configuration, represented by a characteristic dimension l; attitude relative to the fluid, α'; mass, m; mass inertia, I; and elastic bending and torsional rigidity, EI' and GJ', respectively (based on beam theory). The pertinent rate quantities include linear velocity, V; angular velocity, Ω; and periodic oscillations typified by frequency, ω. The pertinent accelerations include linear and angular accelerations, a and $\dot{\Omega}$, respectively. Gravitational effects are characterized by the acceleration of gravity, g. Time, t, and angular displacement of a control surface, δ, are also pertinent parameters. These quantities can be

summarized as

$$F = f(\rho_f, \mu, V_s, l, \alpha', V, a, \delta, \Omega, \dot{\Omega}, \omega, g, t, m, I, EI', GJ') \tag{1a}$$

$$M' = f(\rho_f, \mu, V_s, l, \alpha', V, a, \delta, \Omega, \dot{\Omega}, \omega, g, t, m, I, EI', GJ') \tag{1b}$$

where F is force and M' is moment.

To determine the dependence of the forces and moments on the quantities on the right side of the respective equations, dimensional homogeneity is established through a dimensional analysis. The resulting dimensionless combination of the physical quantities constitutes the similitude requirements for model testing.

Three fundamental units are involved in the mechanics of forces and moments: the unit of length, l; the unit of time, t; and the unit of mass, m. All the quantities in equations (1a) and (1b) can be expressed in terms of these fundamental units, as indicated in table 1.

A dimensional analysis of equations (1a) and (1b) using the Lord Rayleigh method (see appendix) and the dimensions of the physical quantities listed in table 1 results in the following equations in which the force F and moment M' are the stipulated phenomena that have been expressed as aerodynamic coefficients. The aerodynamic coefficients are functions of the fourteen dimensionless parameters, which represent the requirements for complete static and dynamic similitude of the model relative to the airplane.

$$\frac{F}{(1/2)\rho_f V^2 l^2} = f\left(\alpha', \delta, \frac{\Omega l}{V}, \frac{\dot{\Omega} l^2}{V^2}, \frac{al}{V^2}, \frac{\omega l}{V}, \frac{\rho_f V l}{\mu}, \frac{V^2}{lg}, \frac{V}{V_s}, \frac{m}{\rho_f l^3}, \frac{I}{\rho_f l^5}, \frac{EI'}{\rho_f V^2 l^4}, \frac{GJ'}{\rho_f V^2 l^4}, \frac{tV}{l}\right) \tag{2a}$$

$$\frac{M'}{(1/2)\rho_f V^2 l^3} = f\left(\alpha', \delta, \frac{\Omega l}{V}, \frac{\dot{\Omega} l^2}{V^2}, \frac{al}{V^2}, \frac{\omega l}{V}, \frac{\rho_f V l}{\mu}, \frac{V^2}{lg}, \frac{V}{V_s}, \frac{m}{\rho_f l^3}, \frac{I}{\rho_f l^5}, \frac{EI'}{\rho_f V^2 l^4}, \frac{GJ'}{\rho_f V^2 l^4}, \frac{tV}{l}\right) \tag{2b}$$

Table 2 identifies the individual similitude parameters, defines them in general terms, and gives examples of their normally applied definitions. The equations of motion of an airplane, in their customary dimensionless form, are defined in terms of these nondimensional parameters. Thus, for the lift equation,

$$C_L = \frac{m(\ddot{z} + qV + g)}{\bar{q}S} = C_{L_u}\frac{\Delta u}{V} + C_{L_\alpha}\Delta\alpha + C_{L_q}\frac{q\bar{c}}{2V} + C_{L_{\dot{\alpha}}}\frac{\dot{\alpha}\bar{c}}{2V} + C_{L_{\delta_e}}\delta_e + C_{L_{\dot{\delta}_e}}\frac{\dot{\delta}_e\bar{c}}{2V} \tag{3a}$$

where, for dimensional homogeneity,

$$\left.\begin{aligned}
\frac{m(\ddot{z} + qV + g)}{\bar{q}S} &= 2\frac{m}{\rho_f S\bar{c}/2}\left(\frac{\ddot{z}\bar{c}}{2V^2} + \frac{q\bar{c}}{2V} + \frac{g\bar{c}}{2V^2}\right) \\
C_{L_u} &= V(\partial C_L/\partial u) \\
C_{L_\alpha} &= \partial C_L/\partial \alpha \\
C_{L_q} &= \partial C_L/\partial (q\bar{c}/2V) \\
C_{L_{\dot{\alpha}}} &= \partial C_L/\partial (\dot{\alpha}\bar{c}/2V) \\
C_{L_{\delta_e}} &= \partial C_L/\partial \delta_e \\
C_{L_{\dot{\delta}_e}} &= \partial C_L/\partial (\dot{\delta}_e\bar{c}/2V)
\end{aligned}\right\} \tag{3b}$$

For the pitching moment equation,

$$C_m = \frac{I_y\dot{q}}{\bar{q}S\bar{c}} = C_{m_0} + C_{m_u}\frac{\Delta u}{V} + C_{m_\alpha}\Delta\alpha + C_{m_q}\frac{q\bar{c}}{2V} + C_{m_{\dot{\alpha}}}\frac{\dot{\alpha}\bar{c}}{2V} + C_{m_{\delta_e}}\delta_e + C_{m_{\dot{\delta}_e}}\frac{\dot{\delta}_e\bar{c}}{2V} \tag{4a}$$

where

$$\frac{I_y\dot{q}}{\bar{q}S\bar{c}} = 2\left(\frac{I_y}{\rho_f S\bar{c}}\right)\left(\frac{\dot{q}}{V^2}\right) = 2\left(\frac{I_y}{\rho_f S\bar{c}^3}\right)\left(\frac{\dot{q}\bar{c}^2}{V^2}\right) = \left(\frac{I_y}{\rho_f S(\bar{c}/2)^3}\right)\left(\frac{\dot{q}\bar{c}^2}{4V^2}\right) \tag{4b}$$

and where the derivatives of the moment coefficients have the same format as those of the lift coefficient.

Although the reduced linear velocity, $\frac{\Delta u}{V}$, is not included in table 2, it is readily obtained from the product of the reduced linear acceleration and time parameters. Thus,

$$\left[\frac{(\Delta\dot{u})l}{V^2}\right]\frac{tV}{l} = \frac{(\Delta\dot{u})t}{V} = \frac{\Delta u}{V} \tag{5}$$

The equations of motion, as exemplified by equations (3) and (4), include the relative density factor, $\frac{m}{\rho_f S\bar{c}/2}$ (eq. (3b)); relative mass moment of inertia, $\frac{I_y}{\rho_f S(\bar{c}/2)^3}$ (eq. (4b)); aircraft attitude; control surface position; and reduced velocity and acceleration parameters. The force equations also include Froude number, $g\bar{c}/2V^2$ (eq. (3b)). Not evident from the equations of motion is the dependence of the aerodynamic coefficients and their derivatives on Reynolds number, Strouhal number, Mach number, and the aeroelastic bending and torsion parameters.

In the following sections, the implications of several key similitude requirements are discussed.

Reynolds Number

Reynolds number is the ratio of the fluid's inertia forces to the viscous forces in the boundary layer of the fluid. It is an important parameter in determining the dynamic similarity of flow around models and full-scale aircraft. When the model data are obtained at much lower Reynolds numbers than those encountered at full-scale conditions, the inertia forces of the fluid on the model are much lower in proportion to the viscous forces than those on the full-scale airplane. As a consequence, the flow conditions are no longer dynamically similar.

The point of transition from laminar to turbulent flow, the thickness of and velocity in the boundary layer at any streamwise station on a surface, and the angle of attack at which the flow field separates from the surface are all functions of Reynolds number. The boundary-layer (viscous flow) conditions on any configuration affect the drag coefficient throughout the angle of attack range and the maximum lift and stall characteristics of the aircraft. The precise effect depends on the particular airfoil and planform used, and on the interference effects of the fuselage and nacelles or pods.

As Reynolds number increases, the point on the surface along the flow line at which the boundary layer changes from laminar to turbulent moves forward. The precise point or locus of transition is affected by the geometry of the surface or body and by the resulting pressure distribution, surface roughness or waviness, and the magnitude of the velocity fluctuations in the airstream. As a result, it is difficult to extrapolate model test results of natural transition effects obtained in present test facilities to full-scale Reynolds numbers. Efforts are frequently made to simulate flow conditions typical of higher-than-test Reynolds numbers by artificially fixing the transition using strips of roughness particles (grit) or other flow-tripping devices. The test results at several Mach numbers are then extrapolated to full-scale Reynolds numbers.

The effect of Reynolds number on stability derivatives and aerodynamic loads at other than near-stall conditions poses problems that have been recognized only in recent years and are only partly understood. Prior to the mid-1960's, Reynolds number was thought to have little effect in the transonic region where the characteristics of the flow were thought to be primarily determined by Mach number. However, both Reynolds and Mach numbers are important in the transonic region, as was effectively shown during the development of the C-141 airplane. Data were obtained in wind-tunnel tests where the Reynolds number based on mean aerodynamic chord was as high as 8.5×10^6 in the transonic region for both natural and artificial boundary-layer transitions. However, when extrapolated independently, these data offered little guidance in the prediction of full-scale values of approximately 50×10^6. Figure 1 (from ref. 4) shows the variation of C_{m_0} as a function of Reynolds number and free and fixed transition for the C-141 airplane at a Mach number of 0.825. The data for natural and artificial transitions appear to converge with increasing Reynolds number; however, an extrapolation of the results of either technique alone to full scale could produce highly erroneous results. The extrapolation of the convergence point for the two sets of data produced a value of C_{m_0} slightly higher than that obtained from flight data. Such convergence was not achieved in the case of the pitching-moment coefficient, C_m.

Figure 2 (from ref. 4) shows the scale effects on the wing-section pitching-moment coefficient of the C-141 airplane at the 38.9-percent and 63.7-percent semispan stations at transonic conditions. The figure shows model data obtained with the boundary-layer transition free and fixed at 0.10 chord, and with vortex generators at 0.55 chord. (Tests showed that the data obtained with the vortex generators at the 0.55-chord location most nearly duplicated the flight test transition data.) In addition, the figure shows flight results and the extrapolation of the model data that correlates with the flight data. It is evident that in the absence of flight data, extrapolation could produce erroneous results. It should also be noted that in comparisons such as this, aeroelastic effects associated with both flight and wind-tunnel data may be as important as the Reynolds number effects.

Many difficulties associated with the simulation of full-scale Reynolds number conditions in model tests are expected to be alleviated through the development of the National Transonic Facility wind tunnel (refs. 5 and 6). This tunnel is expected to be capable of providing data for Reynolds numbers up to approximately 45.72×10^6 per meter (150×10^6 per foot) and for Mach numbers ranging from 0.2 to 1.2. The facility is based on the cryogenic concept in which low temperatures are used to increase Reynolds number through the reduction of viscous forces. Thus, many of the practical problems of high-pressure test facilities are avoided. Another anticipated capability not attainable in flight or pressure-tunnel tests is the separation of Reynolds number effects from aeroelastic effects.

Mach Number

Mach number, the ratio of vehicle velocity to the velocity of sound of the compressible fluid medium in which the vehicle is flying, is the parameter that assures the similitude of the fluid-compressibility effects on aircraft having geometric similitude. Since the essential characteristic of a compressible fluid is that a change in absolute pressure causes a change in the density of the fluid, the measure of the compressibility of the fluid is the rate of change of pressure with density, $\partial p_f/\partial \rho_f$, at adiabatic (isentropic) conditions. This quantity is equal to the square of the velocity of the propagation of a disturbance in the fluid, $V_s^{\ 2}$. The quantity $\partial p_f/\partial \rho_f$ is also equal to $\gamma(p_f/\rho_f)$ from the adiabatic relation where $p_f(\bar{v})^\gamma$ is a constant. Thus,

$$\partial p_f/\partial \rho_f = V_s^{\ 2} = \gamma(p_f/\rho_f) \tag{6}$$

Applying the above relation to the incompressible-flow equation $\bar{q} = 1/2\rho V^2$, universally used as the reference dynamic pressure in the equations of motion, results in the relation

$$\bar{q} = (1/2)\rho_f\left(\frac{V^2}{V_s^{\ 2}}\right)V_s^{\ 2} = (1/2)\rho_f M^2\left[\gamma(p_f/\rho_f)\right] = (\gamma/2)p_f M^2 \tag{7}$$

or

$$\bar{q}/p_f = (\gamma/2)M^2 = \frac{\text{Fluid inertia force}}{\text{Fluid pressure force}} \tag{8}$$

Hence, equation (7) shows that the reference free-stream dynamic pressure can be expressed as a function of the adiabatic exponent of the fluid, free-stream static pressure, and free-stream Mach number. Equation (8) shows that Mach number indicates the ratio of the fluid's inertia force to its pressure force.

The true stagnation pressure for compressible flow can be obtained from the following expression (ref. 7):

$$\bar{q}_c = \bar{q}\left(1 + 1/4M^2 + \frac{2-\gamma}{24}M^4 + \ldots\right) \tag{9}$$

The corresponding stagnation temperature, as a function of free-stream temperature and Mach number, is obtained from the equation

$$T_0 = T\left(1 + \frac{\gamma-1}{2}M^2\right) \tag{10}$$

Equations (9) and (10) show that the differences in true and incompressible-flow dynamic pressure and temperature are negligible for Mach numbers less than approximately 0.20. Although the free-stream Mach number may be low, significant compressibility effects may be present in the local flow. For example, near the upper surface of a thick wing at high angles of attack, the local Mach number may approach unity even though the free-stream Mach number may be only approximately 0.30.

An interesting example of the effects of the interaction of Mach number and Reynolds number on the crossflow drag of a cylinder in the Mach number range from 0.20 to 0.40 was reported in reference 8. As shown in figure 3 (from ref. 8), at Mach numbers above 0.20 the cylinder drag coefficient peaks at Reynolds numbers between 4×10^6 and 8×10^6 as a function of Mach number, with a critical variation in the drag coefficient occurring at a free-stream Mach number of approximately 0.46. As the Mach number of the flow around the cylinder approaches the critical peak value, the compressibility effect causes the point of flow separation to move forward, resulting in an increase in the drag coefficient. Figure 4(a), which is a cross-plot of figure 3, shows this increase in drag as a function of free-stream Mach number at a Reynolds number of 7.5×10^6. Figure 4(b) shows that at a constant free-stream Mach number, an increase in Reynolds number in the region around 7×10^6 causes a thinning of the boundary layer with a resultant rearward movement of the separation point, a narrowed wake, and, thus, a decrease in drag. These counteractive effects of Mach and Reynolds numbers result in the peaks shown in figure 3. As noted in the reference, for free-stream Mach numbers equal to or greater than the critical Mach number, the adverse compressibility effect on flow separation is considerably greater than the favorable effect of Reynolds number. As a result, large drag increases occur, as shown by the isolated test points in figure 3 for Mach numbers of 0.45 and 0.50.

The compressibility effect on stagnation temperature (eq. (10)) must be considered at high supersonic and hypersonic Mach numbers. When the temperatures at some points in the flow field of the full-size aircraft reach levels that cause significant dissociation, ionization, changes in the adiabatic constant γ, or heat capacity lag, then the temperature effects must be duplicated in the model tests. For example, a model test at a Mach number of 5 and a free-stream temperature of 278 kelvins (500° R) produces a stagnation temperature (as shown by eq. (10)) of 1667 kelvins (3000° R). For these conditions, perfect gas relations should not be assumed.

Mach number effects reach a maximum at a free-stream Mach number of about 5. Near this Mach number, a strong coupling of Mach and viscous effects generally begins. This coupling is associated with the proximity of the shock waves and body surfaces. The shock waves interact extensively with the boundary layer, thereby inducing hypersonic flow conditions. As Mach number is further increased, Mach effects decrease as boundary-layer interaction effects increase. At a Mach number of about 15, the viscosity temperature effects behind the shock wave become significant.

Reduced Angular Velocity and Strouhal Number

Although the reduced angular velocity parameter, $\frac{\Omega l}{V}$, and Strouhal number, $\frac{\omega l}{V}$, are similar in form, they are different. The reduced angular velocity parameter applies to the angular rates of the airplane (p, q, and r) and the control surfaces ($\dot{\delta}_e$, $\dot{\delta}_r$, and $\dot{\delta}_a$). Strouhal number, on the other hand, is related to the oscillatory frequency, ω, of a periodic motion.

The Strouhal number, or reduced frequency parameter, is used to establish similitude for the unsteady flow effects caused by the oscillatory perturbations of the aircraft. Flight data from oscillatory maneuvers should be compared with forced-oscillation wind-tunnel data (ref. 9) obtained at the same or similar Strouhal number and amplitude of oscillation, as well as the same angle of attack, Mach number, and Reynolds number. For flight data from nonoscillatory maneuvers, caution should be used in comparisons with oscillatory wind-tunnel model data. When the flow is separated, results from curved-flow wind-tunnel tests may be required for correlation (ref. 10).

Although reduced angular velocity, $\frac{\Omega l}{V}$, is the proper parameter to apply to the dynamic derivatives (for example, $C_{n_r} = \frac{\partial C_n}{\partial (rb/2V)}$), these derivatives may be significantly affected by unsteady flow effects (Strouhal number), particularly in the case of aircraft with delta and swept wings at high angles of attack where the flow is separated. Where the oscillatory frequency effects are significant, flow separation may cause pronounced changes in the boundary layer, and the time required for the flow to adjust to changing conditions may be appreciable. For the high angle of attack data of figure 5 (from ref. 11), separation effects are largest at low Strouhal numbers and decrease with increasing Strouhal number. For attached flow conditions, changes in attitude have a much smaller effect on the boundary layer, which causes the derivatives to be less dependent on frequency.

The effect of the amplitude of oscillation on the stability derivatives appears to depend substantially on the angle of attack of the wing and the Strouhal number (refs. 9 and 10) as well as the derivative concerned. Figure 5 shows typical effects of the amplitude of oscillation and Strouhal number on the derivatives for yaw damping, directional stability, and effective dihedral for a delta wing at several angles of attack. The combined form of the derivatives shown in figure 5 is a consequence of the phasing of the forces and moments resulting from the perturbed motions of the forced-oscillation technique.

Reduced angular velocity is one of the principal similitude parameters used in spin-tunnel testing to relate the spin characteristics of models and full-scale aircraft. This parameter, which is assumed to be proportional to the tangential velocity, ΩR, of the model about the vertical spin axis divided by the vertical

velocity of the airstream in the tunnel, is normally referred to as the helix angle, γ'. Thus,

$$\gamma' = \tan^{-1} \frac{\Omega R}{V} = f\left(\frac{\Omega l}{V}\right) \tag{11}$$

In spin model tests it is also important to account for differences in Reynolds number (ref. 12). For example, differences in crossflow Reynolds number for the forebodies of long-nose configurations may cause prospin yawing of the model but antispin yawing of the actual airplane.

Froude Number

Froude number, $\frac{V^2}{lg}$, must be duplicated to assure similitude of inertial and gravitational effects on maneuvering vehicles having geometric similitude. The number was originally developed in relation to ship studies to provide a similitude criterion for equating the pressure coefficients, $p_f/\rho_f V^2$, at corresponding points on a ship and its model, and the nondimensional shape of the wave emanating from the hull of the ship and its model. Froude number is significant in the takeoff runs of flying boats, which do not begin to plane until a critical or hump speed (where wave-making resistance is maximum) has been passed. This critical speed, which is a function of Froude number, is determined from model tests.

The physical significance of Froude number as applied to flight is illustrated by the following examples. For a constant-altitude banked turn with an instantaneous radius of turn R and corresponding rate of turn Ω (or $\frac{V}{R}$), the bank angle is given by

$$\Phi = \tan^{-1} \frac{MR\Omega^2}{W} = \tan^{-1} \frac{V^2}{Rg} = f\left(\frac{V^2}{lg}\right) \tag{12}$$

The corresponding normal load factor is expressed as

$$\bar{a}_n = \frac{1}{g}\left[\left(\frac{V^2}{R}\right)^2 + g^2\right]^{1/2} = \left[\left(\frac{V^2}{Rg}\right)^2 + 1\right]^{1/2} = f\left(\frac{V^2}{lg}\right) \tag{13}$$

Thus, to obtain the same load factor and bank angle in a coordinated turn, the model and the full-size airplane must have the same Froude number.

In spin-tunnel tests, a model spinning at an angular rate Ω, having a turning radius R about a vertical axis, and subject to a vertical tunnel velocity V will describe a helix angle (eq. (11)) and be subject to a centrifugal force

$$F = M\Omega^2 R \tag{14}$$

Combining equations (11) and (14),

$$\frac{F}{M} = \frac{V^2}{R}\tan^2 \gamma' \tag{15}$$

which, with R proportional to a representative dimension l of the model, yields

$$\frac{F}{W} = \frac{V^2}{Rg}\tan^2 \gamma' = f\left(\frac{V^2}{lg}, \frac{\Omega l}{V}\right) \tag{16}$$

Thus, the ratio of inertial force to gravitational force in the spin-tunnel test is a function of both Froude number and helix angle (reduced angular rate).

For an airplane in steady, level, 1g flight, the lift coefficient is given by

$$C_L = \frac{W}{1/2\rho_f V^2 S} = 2\left(\frac{m}{\rho_f S\bar{c}}\right)\left(\frac{g\bar{c}}{V^2}\right) = f\left(\frac{m}{\rho_f l^3}, \frac{gl}{V^2}\right) \tag{17}$$

Thus, the similitude requirements for level flight entail both relative density factor and Froude number.

When the airplane is subjected to a pullup maneuver and experiences linear acceleration along the z-axis as well as centrifugal acceleration, the lift equation becomes

$$C_L = \frac{m(\ddot{z} + qV + g)}{1/2\rho_f V^2 S} = 2\left[\frac{m}{\rho_f S(\bar{c}/2)}\right]\left(\frac{\ddot{z}\bar{c}}{2V^2} + \frac{q\bar{c}}{2V} + \frac{g\bar{c}}{2V^2}\right) \tag{18}$$

The similitude requirements now include reduced linear acceleration and reduced angular rate as well as relative density factor and Froude number.

Reconsidering equation (18) in terms of the load factor,

$$C_L = 2\frac{mg\bar{a}_n}{\rho_f V^2 S} = 2\left(\frac{m}{\rho_f S\bar{c}}\right)\left(\frac{g\bar{c}}{V^2}\right)\bar{a}_n \tag{19}$$

Comparison of equations (18) and (19) indicates that the matching of load factor does not imply the matching of Froude number, because $\bar{a}_n$ is given by

$$\bar{a}_n = 2\frac{V^2}{g\bar{c}}\left(\frac{\ddot{z}\bar{c}}{2V^2} + \frac{q\bar{c}}{2V} + \frac{g\bar{c}}{2V^2}\right) \tag{20}$$

Thus, in a pullup maneuver, $\bar{a}_n$ is functionally dependent on three independent similitude parameters.

Froude number similitude requirements for a free-flying model can be readily satisfied if Mach number (compressibility) effects are negligible. If compressibility effects are significant, similitude requirements will include Mach number as well as Froude number and relative density factor, as shown by the following derivation of equation (17).

$$C_L = \frac{W}{1/2\rho_f V^2 S} = 2\frac{mg}{\rho_f M^2 V_s{}^2 S} = 2\frac{m}{\rho_f S\bar{c}}\left(\frac{g\bar{c}}{M^2 V_s{}^2}\right) = f\left(\frac{m}{\rho_f l^3}, M, \frac{V^2}{lg}\right) \tag{21}$$

Because of the velocity constraint imposed by Mach number similitude for compressible flow conditions, free-flight model simulation of a full-scale airplane satisfying Mach number and relative density factor similitude would require that the atmospheric gravitational field be scaled to satisfy Froude number similitude. Since such scaling is not possible, Froude number similitude can be achieved only under limited geometric-scale conditions, and thus, the model would normally be flown at a different angle of attack than the full-scale airplane.

Although practical only in dynamic wind-tunnel testing, one approach to satisfying similitude requirements for Mach, Froude, and Reynolds numbers for a free-flying model and the full-scale airplane is to fly the model in a pressurized wind tunnel that uses a particular refrigerant as the fluid medium. As indicated in reference 13, the velocity of sound in this refrigerant is approximately half that in air, and its density is about four times that of air with little difference in absolute viscosity. To attain Mach number, Froude number, and Reynolds number similitude for a full-scale airplane at sea level would require a 1/4-scale model if the density of this refrigerant were increased to eight times atmospheric density by pressurizing the gas to two atmospheres at normal ambient temperature.

Relative Density Factor and Relative Mass Moments of Inertia

In the preceding discussion on Froude number, the relative density factor, $\frac{m}{\rho_f l^3}$, was shown to be a basic similitude parameter in the aerodynamic force equations. This factor is important in model studies of flutter as well as those of stability and control characteristics.

The relative mass moment of inertia parameter, $\frac{I}{\rho_f l^5}$, has the same significance for the moment equations as the relative density factor has for the force equations. Thus, when the equation

$$I_y\dot{q} = C_m 1/2\rho_f V^2 S\bar{c} \tag{22}$$

is transposed and $\dot{q}$ is stated in nondimensional format, the moment coefficient is given as

$$C_m = 2\left(\frac{I_y}{\rho_f S\bar{c}}\right)\left(\frac{\dot{q}}{V^2}\right) = 2\left(\frac{I_y}{\rho_f S\bar{c}^3}\right)\left(\frac{\dot{q}\bar{c}^2}{V^2}\right) = f\left(\frac{I_y}{\rho_f l^5}, \frac{\dot{\Omega} l^2}{V^2}\right) \tag{23}$$

or

$$C_m = f\left[\frac{m}{\rho_f l^3}, \left(\frac{k}{l}\right)^2, \frac{\dot{\Omega} l^2}{V^2}\right] \tag{24}$$

For the model to have the same moment coefficient as the full-scale airplane, the relative mass moment of inertia parameters, $\frac{I}{\rho_f l^5}$, and the reduced angular accelerations, $\frac{\dot{\Omega} l^2}{V^2}$, must be identical. For a rigid airplane, mass moment of inertia characteristics (including products of inertia) can be simulated on the model by the appropriate distribution of several masses to provide the same reduced radius of gyration, k/l, as on the airplane, assuming that the relative density factor, $\frac{m}{\rho_f l^3}$, is also satisfied. For a flexible airplane, similitude of actual mass distribution would be required for the flying model to provide similitude of maneuvering inertial load distribution and elastic deformations.

Aeroelastic Bending and Torsion Parameters

When the aerodynamic characteristics are affected by the flexibility of any component part of the airplane, the required elastic similitude of the model and the airplane is provided by the aeroelastic-bending and aeroelastic-torsion parameters, $\frac{EI'}{\rho_f V^2 l^4}$ and $\frac{GJ'}{\rho_f V^2 l^4}$, respectively. These can also be expressed as $\frac{EI'}{\bar{q} l^4}$ and $\frac{GJ'}{\bar{q} l^4}$. In addition to elastic similitude, the similitude requirements for the relative mass density factor, $\frac{m}{\rho_f l^3}$, relative mass moments of inertia, $\frac{I}{\rho_f l^5}$, and attitude, α and β, must be met to assure the similitude of inertial and aerodynamic load distribution for the same Mach number, if compressibility is involved, or scaled velocity, if compressibility is not a factor (low-speed flight). If partially separated flow is a factor in the simulation, the Reynolds number must be given careful consideration.

If all the preceding conditions are satisfied, the aeroelastic airplane will be properly simulated by the model for free-flight and flutter tests. However, when compressibility effects are a factor, the model must be flown at full-scale Mach

number, and, as a consequence, Froude number similitude cannot be satisfied except for the limited free-flight test conditions mentioned previously. Therefore, in general the model will be flown at a different angle of attack than the full-scale aircraft. Thus, the aeroelastic deformations will not be representative of the full-scale airplane, except as noted.

In the wind-tunnel testing of a mounted elastic model, there are several limitations that affect the data. These limitations are discussed later in this report and in reference 14.

Variation of the angle of attack of an airplane at constant dynamic pressure implies a variation in load factor and, thus, a variation in mass inertial loading that affects the elastic deformation and therefore the aerodynamic loading of the airplane. In static, mounted-model wind-tunnel tests, the structural flexibility of the model combined with a specific dynamic pressure represents a specific load factor on the full-scale airplane. Dynamic pressure must be varied (at the expense of Reynolds number) with angle of attack to simulate the deformation due to inertial mass and structural flexibility in the full-scale airplane.

MODEL TEST TECHNIQUES AND SCALE FACTORS

To obtain model data that are directly applicable to the full-size airplane, the model test conditions must be scaled, on the basis of the scale of the model, to satisfy the similitude requirements discussed previously. Scaling of the model implies geometric scaling in every respect, including the gaps between the control surfaces and the adjacent structure, and protuberances. Both the techniques and the objectives must be considered to determine which similitude parameters are pertinent to the test. The two general categories of test techniques are the mounted-model and free-flying-model techniques.

All test techniques and objectives require Reynolds number similitude to provide duplication of the transition from laminar to turbulent boundary layer flow, proper scaling of boundary layer thickness, duplication of partially separated flow conditions, and duplication of possible effects of the interaction of Reynolds number and Mach number, as discussed earlier. In addition, all test techniques and objectives require that angle of attack, angle of sideslip, and control surface positions be duplicated.

Individual test techniques and the related scaling of the model test conditions (scaling factors) and reduction of data in light of similitude requirements are discussed in the following sections. Scaling factors for mounted and free-flying models are summarized in tables 3 and 4, respectively.

Mounted Wind-Tunnel Models

Mounted-model testing, which eliminates the need to consider Froude number, is a practically universal wind-tunnel technique. For rigid models, this

test technique has versatility, providing static and dynamic characteristics as functions of angle of attack, angle of sideslip, Reynolds number, and Mach number. The characteristics thus obtained for the rigid model are due to flow fields and air loadings that are not influenced by inertial loadings. Thus, the data are considered to be zero-mass data directly applicable to the conventional rigid-body equations of motion in which inertial loads and moments are accounted for by the inertia terms.

For mounted aeroelastic models, there are two categories of testing: (1) static tests to determine aeroelastic effects on performance and stability and control characteristics as a function of angle of attack, and (2) dynamic tests to determine flutter characteristics. The static tests are complicated by the fact that the model must be properly scaled for mass, mass distribution, and elasticity to simulate and provide data for selected load factor, airplane-to-tunnel dynamic pressure ratio, and Mach number conditions. Data obtained during the tests for other than selected design conditions must be manipulated theoretically to provide corrected predictions that properly account for aeroelastic deformation effects. For models constructed for flutter tests, mass distribution must also be properly scaled to account for inertial effects.

Rigid models. - Scaling factors for model-to-airplane parametric ratios to satisfy similitude requirements in static and dynamic tests of mounted and restrained models for incompressible and compressible flow are summarized in table 3(a). Incompressible-flow static test similitude requires geometric scaling of the model and duplication of the angle of attack, angle of sideslip, control surface positions, and Reynolds number. For compressible flow, Mach number must also be duplicated.

For incompressible flow, when test facilities permit, the range of Reynolds numbers anticipated for the full-scale airplane is obtained in the model test by varying the wind-tunnel kinematic viscosity and velocity in accordance with the following relation (from table 3(a)) for Reynolds number similitude.

$$\frac{V_m}{\nu_m} = \frac{V_A}{\nu_A} n^{-1} \tag{25a}$$

For compressible flow, because of the restraint of Mach number similitude on velocity, the above equation is modified to

$$\frac{V_{s_m}}{\nu_m} = \frac{V_{s_A}}{\nu_A} n^{-1} \tag{25b}$$

where V_s is the velocity of sound.

When wind-tunnel variables do not permit the above conditions to be satisfied, Reynolds number similitude for both incompressible and compressible

flow can sometimes be approximated by fixing the transition on the model's lifting surfaces. This technique to achieve Reynolds number is not foolproof, as was discussed in the section on the similitude requirements for Reynolds number.

In addition to the requirements for static tests, tests to obtain dynamic aerodynamic characteristics require reduced angular rate similitude (table 3(a)). Dynamic testing techniques employing curved flow (ref. 10) or rotary flow (ref. 13) relative to a stationary model are limited to incompressible flow conditions. The test procedure most commonly used for both incompressible and compressible flow uses a model that is either rotating (ref. 15) or oscillating (refs. 9 and 10) in a linear stream.

In using the curved-flow technique for a fixed-flow velocity, the curvature of the sidewalls of the test section is varied to provide various angular rates of flow, Ω. For longitudinal tests where the y-axis of the model is vertical, Ω is equivalent to the pitch rate, q, and both C_m and C_L are obtained as functions of reduced angular rate, $\frac{q\bar{c}}{2V}$ (tables 2 and 3(a)), for each of a number of angles of attack. From reduced angular rate, C_{m_q} and C_{L_q} are obtained as functions of angle of attack. With the y-axis of the model horizontal, Ω is equivalent to yaw rate, r, and both C_n and C_l are obtained as functions of reduced angular rate, $\frac{rb}{2V}$, from which C_{n_r} and C_{l_r} are obtained as functions of angle of attack.

In the rotating-flow technique, the flow is rotated through a cylindrical test section at an angular rate Ω and an axial velocity V. This technique provides C_l and C_n as functions of $\frac{pb}{2V}$ and angle of attack.

In the rotating-model technique, the flow is linear, and may be compressible, and the model is rotated at an angular rate Ω. The technique provides the same results as obtained from the rotating-flow technique but has the added versatility of variable Mach number.

In the forced-oscillation technique, the model is oscillated about the pitch, roll, or yaw axis at various frequencies, ω, and amplitudes, φ'_0, at each of several angles of attack to assure data coverage for similitude in attitude, displacement, reduced angular rate, and Strouhal number. The flow stream may be compressible or incompressible (tables 2 and 3(a)). Since the amplitude of the angular rate Ω is equal to $\varphi'_0\omega$, the reduced angular rate $\frac{\Omega l}{V}$ is equal to $\frac{\varphi'_0\omega l}{V}$. Therefore,

$$\frac{\Omega l}{V} = f\left(\varphi'_0, \frac{\omega l}{V}\right) = f\left(\varphi'_0, N_{Str}\right) \tag{26}$$

Dynamic derivatives obtained from curved-flow, rotating-flow, or rotating-model techniques will not necessarily be the same as those obtained from the oscillatory technique. As shown in reference 9, the oscillatory technique yields compounded derivative values (that is, $C_{n_r} - C_{n_{\dot{\beta}}}$ rather than C_{n_r}). The differences become more pronounced under partially separated flow conditions at high angles of attack where amplitude and oscillatory frequency affect the flow field around the separated area (fig. 5). The application of oscillatory model data to full-scale conditions may therefore be questionable where large differences exist between model and full-scale Reynolds numbers.

Aeroelastic models. - As mentioned earlier, there are two categories of aeroelastic-model testing: (1) static tests to determine aeroelastic effects on performance and stability and control characteristics, and (2) dynamic tests to determine flutter characteristics. Normally, the model used for dynamic flutter tests cannot be used for static tests because of its fragile structural design. This fragileness results from the fact that the mass and mass distribution scaling of the model is designed for the limited fluid density changes obtainable in the test facility where full-scale dynamic pressure and Mach number are simulated. Therefore, static tests in such instances are normally conducted with another model properly scaled for stiffness characteristics but not scaled for mass. In test facilities that permit large changes in density ratio, ρ_{f_m}/ρ_{f_A} (such as a variable pressure tunnel using a particular refrigerant), scaled mass and mass distribution can be obtained along with scaled bending and torsional stiffness. A single model sturdy enough for both dynamic and static tests can then be used. Pertinent scaling factors from table 3(b) for the same Mach conditions are as follows:

$$m_m = \left(\rho_{f_m}/\rho_{f_A}\right) n^3 m_A \tag{27}$$

$$I_m = \left(\rho_{f_m}/\rho_{f_A}\right) n^5 m_A \tag{28}$$

$$\frac{(EI')_m}{(EI')_A} = \frac{(GJ')_m}{(GJ')_A} = \frac{\bar{q}_m}{\bar{q}_A} n^4 \tag{29}$$

Much flutter testing is performed in wind tunnels using cantilevered models of aircraft structures such as the wing, tail, or empennage. These tests rely on the separation of flutter mode frequencies and the unmodeled aircraft rigid mode frequencies to achieve similitude. In flutter tests of complete models, the model is mounted with spring-restrained freedom in vertical movement as well as pitch, roll, and yaw. The resonant frequencies of the mount system are very low relative to the model flutter frequencies, which minimizes the contamination of the flutter data with mount effects. During the test, at any given Mach number and angle of attack, the tunnel dynamic pressure is increased to the point where incipient

flutter is encountered. Since the model is designed for a fixed dynamic pressure ratio, $\bar{q}_m/\bar{q}_A$, the airplane dynamic pressure and pressure altitude for the flutter characteristics are readily obtained from the tunnel dynamic pressure and Mach number. Using the Strouhal number similitude parameter (table 3(b)), the airplane flutter frequency is found to be

$$\omega_A = \omega_m R_{V_s} n^{-1} = \omega_m \frac{V_{s_m}}{V_{s_A}} n^{-1} \tag{30}$$

For static tests, the fulfillment of aeroelastic-bending and -torsion similitude requirements (eq. (29)) is of prime concern in providing scaled bending and torsional deformation due to airloads. Although desirable, scaling of mass and mass distribution is not as important because the data from mounted-model tests must be corrected for inertial effects.

The static aeroelastic model is normally designed to simulate the airplane at its cruise Mach number and dynamic pressure. Wind-tunnel tests are conducted at the cruise Mach number but are limited to available tunnel dynamic pressures. Thus, the ratio $\bar{q}_m/\bar{q}_A$ and model scale n are fixed, and, as a consequence, the stiffness ratios (eq. (29)) are also fixed. When tested at the cruise Mach number and scaled cruise dynamic pressure over an angle of attack range, the model provides static longitudinal data (C_L and C_m) that have the correct slope with respect to angle of attack for the $1g$ environment of the wind tunnel. If mass and mass distribution are properly scaled, the α and C_m corresponding to the cruise C_L point in the data will be the only representative data for the cruise Mach number. All other C_L and C_m data points at the test Mach number will require correction for inertial effects since they will be for other than $1g$ conditions at the cruise dynamic pressure and Mach number.

Aeroelastic-model testing procedures for design and off-design conditions are discussed in detail in reference 14. In addition, the reference includes detailed information regarding correction of the data.

Free-Flying Models

Small-scale free-flying models are an important means of determining (1) the dynamic behavior of airplanes at angles of attack up to and including stall, (2) configuration changes necessary to improve stability and control characteristics relatively inexpensively and quickly, (3) spin characteristics and recovery techniques, (4) gust alleviation techniques to extend the fatigue life of the airplane structure, and (5) methods for evaluating and improving control systems to develop new concepts (such as control-configured vehicles). The smallest of these free-flight models, such as spin-tunnel models, have no instrumentation; the larger models, such as the wind-tunnel free-flight models and small-scale drop

models, carry instrumentation for measurement of flight variables. Tests of the small-scale models are recorded on motion pictures. These models are usually suitable for mounting in wind tunnels to provide force data.

The complexity of many new configuration concepts has necessitated the use of large-scale models. Such models employ remote-pilot control and thus can perform many hazardous maneuvers (such as stall, departure, and spin) that are normally avoided in full-scale testing.

Whether or not a free-flying model can provide adequate static and dynamic simulation depends on the extent to which similitude conditions can be satisfied. For incompressible flow, the models are Froude scaled to provide Froude number similitude and thus assure similitude of inertial and gravitational effects during maneuvers as well as during steady-state flight. Where compressibility is a factor, the models, flown at full-scale Mach number, are Mach scaled. Mach-scaled models generally do not satisfy Froude number similitude and hence do not satisfy angle of attack similitude. The scaling factors for each type of scaling are summarized in table 4. Scaling is discussed in more detail later in this report.

In order of their development, the free-flying models in current use are spin-tunnel models, wind-tunnel models, small-scale drop models, and large-scale models. The test techniques using these models are discussed briefly in the following sections.

Spin-tunnel models. - The earliest use of free-flight models was in the study of spin characteristics. The simplest test technique was to drop a small model in a spinning attitude from a height of about 30.5 meters (100 feet) and take motion pictures of its descent (ref. 16). This elementary approach was subsequently replaced by tests conducted in the Langley 15-Foot Spin Tunnel (ref. 17).

The present Langley 20-Foot Vertical Spin Tunnel (ref. 12), which replaced the 15-Foot Spin Tunnel, is a vertical return-flow tunnel with the air drawn upward by a propeller located at the top of the tunnel. The maximum velocity attainable is 29.6 meters per second (97 feet per second) with a corresponding maximum Reynolds number of 0.18×10^6 per meter (0.6×10^6 per foot). The air can be accelerated or decelerated rapidly. The model is kept near the center of the tunnel at the desired height in the test section to facilitate visual study as well as the photographing of the fully developed spin and the recovery from spin.

The models are normally of rigid fiber glass construction and are Froude scaled (table 4). The geometric scale, n, varies from approximately 1/10 to 1/40, and Reynolds numbers vary from approximately 0.05×10^6 to 0.20×10^6 based on the wing chord. In spite of the large difference between full-scale and model-scale values of Reynolds number, the spin-tunnel model results are representative of full-scale conditions for flow over the lifting surfaces and provide good predictions of the full-scale spin characteristics. Data from force tests have shown that there is little or no Reynolds number effect on lift at spinning attitudes. However, the crossflow effects on the forward section of the fuselage may significantly influence the spin, especially for long-nosed military fighter aircraft

(ref. 18). Strakes are often used on the forebody of the model to induce full-scale crossflow effects in the low Reynolds number tests.

The models are hand launched in both steep and flat attitudes to obtain all the spin modes possible with the configuration. The model seeks its natural developed spin modes at angles of attack above stall. The aerodynamic controls are deflected remotely to predetermined positions for recovery.

Model spin results and full-scale flight data are continually correlated and filed for reference. These correlations provide the experience and knowledge necessary to properly evaluate the model results (ref. 19).

Wind-tunnel free-flying models. - The testing of free-flight models in a conventional wind tunnel is primarily intended to obtain a qualitative evaluation of dynamic stability and control characteristics for the full angle of attack range, which includes stall. This type of testing, originally performed in small-scale tunnels (ref. 20), is currently conducted in the Langley Full-Scale Tunnel, which has an open throat test section with a height of 9.14 meters (30 feet) and a width of 18.28 meters (60 feet), and provides airspeeds from 0 to 48.75 meters per second (0 to 160 feet per second). The test models are powered by compressed air and flown in 1g level flight. By careful control of tunnel airspeed, model trim, and model thrust, the models can be flown at angles of attack ranging from low to stall in a single, continuous test sequence. The large test section provides the model controllers with an unobstructed view of the model during the tests.

The models tested are normally rigid, Froude-scaled replicas of the full-scale aircraft. Their geometric scales vary from 1/10 to 1/6 of the typical full-scale maneuvering airplanes, which results in models with lengths of about 2.1 meters (7 feet), wingspans of 1.52 to 1.83 meters (5 to 6 feet), and weights of 224 to 267 newtons (50 to 70 pounds). Such scaling, as noted in table 4, produces model angular motions that are as much as three times as fast as those of the full-scale airplane; therefore, several pilots are required to handle the piloting task. Since the test section of the tunnel operates at an air density near that at sea level, the ratio of the tunnel air density to that of the test altitude of the full-scale airplane must be considered in the scaling of the model.

The test setup for this technique is illustrated in figure 6. The model is flown remotely without restraint by two pilots, one controlling the longitudinal motions and the other the lateral-directional motions. The model thrust is controlled independently by a third operator.

A light, flexible umbilical cable is used to supply the model with compressed air, electrical power, and pilot control signals as well as to catch the model when a test is terminated or when uncontrolled motions occur. The cable is kept slack during the tests by a safety-cable operator.

The model is instrumented to measure linear accelerations, body-axes angular rates, and control-surface positions which are transmitted by way of the

flight cable to strip chart recorders. Motion pictures are taken from several advantageous positions. A ground-based minicomputer provides the desired representation of automatic stability and control augmentation systems.

Although it is possible for a single pilot to fly the model, such an arrangement is not suitable for research purposes because the pilot would have to concentrate intently on keeping the model in flight and at the same time evaluate its flight characteristics in detail. Because the model angular rates are high, considerable piloting skill is required. In addition, when flying a model by remote control, the pilot must fly with only visual cues since he cannot sense accelerations as he does in a real airplane. The lack of motion cues often results in delayed control inputs, which can be significant when attempting to fly a model in a relatively restricted test section at high angles of attack where the motions are lightly damped. Therefore, each pilot concentrates on one mode of oscillation only. The quick-response control surface actuators provide the pilot with relatively tight control.

Typical investigations include dynamic stability and control studies, including augmentation requirements, at angles of attack up to stall, and the evaluation of pilot control techniques. A representative flight test involving a model of the XB-58 airplane is discussed in reference 21. Typical differences between the characteristics of the model and the full-scale airplane due to differences in Reynolds number are discussed in the reference.

Small-scale drop models. - Wind-tunnel free-flight tests permit observance of the dynamic characteristics at angles of attack up to stall, including divergence. Spin-tunnel tests provide information regarding full-spin and recovery characteristics. However, for the study of the transient motions that occur from the onset of stall until a spin is fully developed, the use of small radio-controlled outdoor models is particularly advantageous. This technique is valuable in determining why aircraft of some designs enter spins more readily than others or are more difficult to recover. The information obtained with free-flight models for the post-stall and spin-entry regimes provides a necessary supplement to the results from spin and conventional wind-tunnel studies.

For the Langley drop-model technique (ref. 22), unpowered models are launched from a helicopter (fig. 7). The altitude at which the model is dropped depends on the launch technique employed. In one technique (ref. 23), the model is either released from the helicopter into a forward gliding flight at an altitude of about 915 meters (3000 feet) and an airspeed just below the stall speed of the model, or it is rotated and launched in a spinning attitude while the helicopter is hovering. In a more commonly used technique (ref. 24), the model is trimmed for approximately zero lift and launched from an altitude of about 1525 meters (5000 feet) and an airspeed of about 40 knots. The model is then allowed to dive for about 5 seconds, after which it is maneuvered by remote control into the stall region, where various control manipulations are used to study pertinent aspects of the test. When the model has descended to an altitude of about 183 meters (600 feet), a recovery parachute is deployed.

Drop models are normally 1/7 to 1/9 scale and are constructed of fiber glass to withstand high landing-impact loads. The models are Froude scaled to simulate the actual airplane at an altitude of approximately 9150 meters (30,000 feet). Since mass scaling is a function of air density ratio, ρ_{f_m}/ρ_{f_A}, and n^3 (table 4), the models are relatively heavy, weighing up to approximately 890 newtons (200 pounds) for high density airplanes. The models are equipped with electrically powered, proportional actuators for operation of the control surfaces and deployment of the recovery parachute. Model velocity, angle of attack, angle of sideslip, control-surface positions, linear accelerations, and the three-axes angular rates are telemetered to the ground from onboard instrumentation. The models are controlled from two ground stations manned by separate pilots and equipped with separate communication systems, motorized tracking units, and telephoto cameras (fig. 8).

Reference 25 discusses drop-model studies of an automatic spin-prevention concept based on the automatic activation of control surfaces when the airplane crosses a threshold defined in terms of angle of attack and yaw rate.

Large-scale models. - In recent years, flight evaluations of high-risk technologies, particularly as applied to highly maneuverable aircraft, have been conducted on large-scale remotely controlled models. Using this technique, the cost and risks of such studies, as well as the time required, can be minimized. This approach, which was developed at the NASA Dryden Flight Research Center, uses both powered and unpowered models. The models are approximately 3/8 scale or larger and have a complete set of stability and control instrumentation.

Data are transmitted by way of a pulse code modulation (PCM) telemetry downlink to the ground station, displayed on the ground cockpit instrument panel, recorded on analog strip charts for flight monitoring, and made available to the ground computer. The ground computer, which contains control laws for augmented control systems, generates control signals based on the telemetered motion variables and the pilot's inputs (from the ground cockpit). These control signals are transmitted to the model through the telemetry uplink (refs. 26 and 27). Scaled dynamic responses are controlled by a single ground-based test pilot who is flying the model from his simulated cockpit.

Reference 28 reports some initial results from flight tests of an unpowered 3/8-scale model (Froude scaled) launched from a B-52 airplane at an altitude of 13,714 meters (45,000 feet) and a Mach number of 0.65. Flight data were obtained over a wide range of conditions in a relatively short time using normal piloting techniques. References 27 and 29 show that through the use of a remotely augmented flight control system, control laws can be readily varied without changing flight hardware.

Since large-scale powered models can be flown at both high and low speeds, special attention must be given to both Froude and Mach scaling.

SCALING LAWS USED FOR MODEL TESTING

In this section, scaling procedures are illustrated for the incompressible and compressible flow test conditions of the free-flying model. For incompressible flow, the kinematic properties are preserved by using velocities scaled from Froude number similitude requirements (Froude scaling). For compressible flow, the compressibility effects are preserved through adherence to Mach number similitude requirements (Mach scaling). To facilitate the assessment of the scaling requirements and the extent to which the requirements are satisfied, Froude- and Mach-scaled nomographs are presented (figs. 9 to 16). The atmospheric characteristics used in formulating the nomographs are from reference 30.

Froude Scaling

As an example in the use of the Froude-scaled nomographs, assume that a 1/2-scale model of a 77,844-newton (17,500-pound) high performance airplane having a wing area of 56 square meters (600 square feet) is to be built on the basis of Froude scaling. Assume that calculations have shown that such a model, complete with propulsion system, radio control, and instrumentation, will result in a model-to-airplane mass ratio, m_m/m_A, of 0.3. Although the stability and control characteristics are of concern in the proposed flight program, the evaluation of the stall, departure, and spin recovery characteristics in the clean configuration is the primary objective. The predicted $C_{L_{max}}$ is 1.2.

Starting from the lower left-hand plot of figure 9 and assuming an n of 0.5 and an m_m/m_A of 0.3, it can be readily determined that to obtain relative density factor similitude, the air density ratio, ρ_{f_m}/ρ_{f_A}, must be 2.4, which establishes the relationship between the model test altitude and airplane altitude. By following the tracer lines for this example, the following additional required scale factors are determined:

$$I_m/I_A = 0.075$$

$$\bar{q}_m/\bar{q}_A = 1.2$$

$$\frac{(EI')_m}{(EI')_A} = \frac{(GJ')_m}{(GJ')_A} = 0.075$$

In addition, based on a ρ_m/ρ_A of 2.4, the simulated airplane altitude for each of several model altitudes can be determined from the lower right-hand plot of figure 9. Using these data and figure 10, the following table of Mach number and Reynolds number ratios can be constructed.

Model altitude, m (ft)	Simulated airplane altitude, m (ft)	M_A/M_m	$(N_{Re})_m/(N_{Re})_A$
3,000 (9,843)	10,680 (35,040)	0.64	0.72
6,000 (19,685)	12,795 (42,040)	0.66	0.76
9,000 (29,528)	15,045 (49,360)	0.68	0.80
12,000 (39,370)	17,500 (57,480)	0.71	0.82
15,000 (49,213)	20,445 (67,070)	0.71	0.85

The data in the above table indicate that for this Froude-scaled model, Reynolds number similitude is not possible at any test altitude, although the difference may not be significant. In addition, the lack of Mach number similitude may result in model data that are not fully representative of the full-scale airplane. In this respect, consider the airplane stall condition ($C_{L_{max}} = 1.2$) that governs the lowest flight velocity. For this condition, the following relationships are obtained.

Model altitude, m (ft)	Airplane altitude, m (ft)	V_A, m/sec (ft/sec)	$V_m = V_A(n)^{1/2}$, m/sec (ft/sec)	M_A	$M_m = M_A\left(\frac{M_m}{M_A}\right)$
3,000 (9,843)	10,680 (35,040)	76.5 (251)	54.1 (177)	0.258	0.165
6,000 (19,685)	12,800 (42,040)	90.5 (297)	64.1 (210)	0.308	0.203
9,000 (29,528)	15,040 (49,360)	104.0 (341)	73.5 (242)	0.356	0.242
12,000 (39,370)	17,500 (57,480)	130.0 (428)	91.9 (303)	0.438	0.311
15,000 (49,213)	20,440 (67,080)	164.0 (538)	116.0 (379)	0.554	0.393

These data show that Mach effects tend to be more significant with increasing test altitude in comparing model data with full-scale results.

To determine the mass ratio and simulated test altitudes that will provide Reynolds number similitude for the Froude-scaled 1/2-scale model, the tracing is started from the upper left-hand plot of figure 10 with $(N_{Re})_m/(N_{Re})_A$ equal to 1 and n equal to 0.5. Thus, at a model test altitude of 9000 meters (29,528 feet), the simulated airplane altitude and Mach number ratio will be 16,350 meters (53,640 feet) and 0.682, respectively. Using the lower right-hand plot of figure 9 and tracing to the left from the point where the model and airplane altitudes intersect, the mass ratio, m_m/m_A, is determined to be 0.370.

Mach Scaling

The tracing of the Mach-scaled nomographs (figs. 11 and 12) for Mach-scaled models ($M_m/M_A = 1$) is similar to that explained for the Froude-scaled nomographs. In applying the nomographs, it can be seen that Froude number ratios, $(N_{Fr})_m/(N_{Fr})_A$, based on the actual gravitational field, are generally

significantly different from unity. As a result of this lack of Froude number similitude in Mach scaling, the model lift coefficient (and hence, angle of attack) is correspondingly different from that of the full-scale airplane. This is indicated more directly by the following relationship.

$$\frac{(C_L)_m}{(C_L)_A} = \left(\frac{m_m g_m}{\bar{q}_m S_m}\right)\Bigg/\left(\frac{m_A g_A}{\bar{q}_A S_A}\right) = \left(\frac{\bar{q}_A S_A}{\bar{q}_m S_m}\right)\left(\frac{m_m g_m}{m_A g_A}\right) \tag{31a}$$

Substituting the Mach-scaled scaling factors from table 4,

$$\frac{(C_L)_m}{(C_L)_A} = \left(\frac{1}{\frac{\rho_{f_m}}{\rho_{f_A}} R_{V_s}^{\ 2}} \cdot \frac{1}{n^2}\right)\left(\frac{\rho_{f_m}}{\rho_{f_A}} n^3 \frac{g_m}{g_A}\right) \tag{31b}$$

or

$$\frac{(C_L)_m}{(C_L)_A} = \frac{\left(C_{L_\alpha}\right)_m}{\left(C_{L_\alpha}\right)_A} \cdot \frac{\alpha_m}{\alpha_A} = \frac{n}{R_{V_s}^{\ 2}} \cdot \frac{g_m}{g_A} \tag{31c}$$

Since Froude number similitude in Mach scaling requires that the model gravitational field g_m vary as a function of $g_A \frac{R_{V_s}^{\ 2}}{n}$, and since this is not possible in atmospheric flight because g_m is equal to g_A, in general it will not be possible for α_m/α_A and $(\delta_e)_m/(\delta_e)_A$ to be unity. One exception is when the model is sized such that n is equal to $R_{V_s}^{\ 2}$. However, except for this special case, the model will be at a lower angle of attack and lift coefficient than the full-scale airplane while flying at the same Mach number. Correspondingly, the C_D and C_m similitude requirements will not be fulfilled. Hence, the performance parameters C_L and C_D from the model data will not be representative of the full-scale airplane.

Another factor to be considered is that bending and torsional stiffness are dependent on the dynamic pressure ratio, $(\rho_{f_m}/\rho_{f_A})R_{V_s}^{\ 2}$, as well as model scale,

whereas mass and mass-moment-of-inertia ratios are dependent on ρ_{f_m}/ρ_{f_A} and model scale only (table 4). Thus, where aeroelastic effects are pertinent, the model testing must satisfy ρ_{f_m}/ρ_{f_A} and dynamic pressure constraints. The nomograph in figure 11 is useful in this respect.

Although Mach scaling provides the correct scaled relationships for obtaining dynamic force and moment coefficients and derivatives, these data presuppose angle of attack similitude. Hence, for the dynamic stability and control derivatives that are sensitive to angle of attack and aeroelastic effects, the model results will not be representative of the full-scale airplane.

CONCLUDING REMARKS

This report has provided a comprehensive review of the similitude requirements and scaling relationships that apply to wind-tunnel and free-flight model airplane testing. These requirements and relationships were considered in relation to test techniques, test conditions (including supersonic flow), and test objectives. The limitations of the test techniques were discussed with emphasis on the free-flying model. Limited comparisons of typical model and full-scale results were also presented.

Particular emphasis was placed on the scaling problems and limitations associated with atmospheric flight tests of large-scale models for compressible flow conditions. It was shown that conventional Mach scaling may be inadequate for simulating the stability, control, and handling qualities characteristics of the actual airplane because of the inability to satisfy Froude number similitude requirements for steady 1*g* flight test conditions. Because of this deficiency, the model data based on Mach scaling may not be representative of the actual airplane for stability and control derivatives that are sensitive to angle of attack and aeroelastic effects.

Dryden Flight Research Center
National Aeronautics and Space Administration
Edwards, Calif., May 23, 1978

APPENDIX—REQUIREMENTS FOR DIMENSIONAL HOMOGENEITY

The dependence of one physical quantity, such as a force or moment, on a number of other physical quantities, and the requirements for dimensional homogeneity in physical equations can be determined using the method of Lord Rayleigh (ref. 31).

In equation (1a), the force F was given to be dependent on a number of other physical quantities. To establish the dimensional homogeneity requirements and the dependence of the force on the other quantities, each physical quantity on the right side of the equation is represented as a power product where the exponents a', b', c', and so forth are to be determined.

$$F = \rho_f^{a'} \mu^{b'} V_s^{c'} l^{d'} (\alpha')^{e'} V^{f'} a^{g'} \delta^{h'} \Omega^{i'} \dot{\Omega}^{j'} \omega^{k'} g^{l'} t^{m'} m^{n'} I^{p'} (EI')^{q'} (GJ')^{r'} \tag{32}$$

In addition, each physical quantity in the equation is expressed in terms of its fundamental units (from table 1).

$$\begin{aligned} mlt^{-2} = {} & (ml^{-3})^{a'} (ml^{-1}t^{-1})^{b'} (lt^{-1})^{c'} (l)^{d'} (1)^{e'} (lt^{-1})^{f'} (lt^{-2})^{g'} (1)^{h'} (t^{-1})^{i'} \\ & (t^{-2})^{j'} (t^{-1})^{k'} (lt^{-2})^{l'} (t)^{m'} (m)^{n'} (ml^2)^{p'} (ml^3t^{-2})^{q'} (ml^3t^{-2})^{r'} \end{aligned} \tag{33}$$

On the basis of the pi theorem of dimensional analysis, the sum of the exponents for each of the fundamental units (m, l, and t) on one side of equation (33) must be equal to the sum of those on the other side. Hence, from equation (33),

$$m: \quad 1 = a' + b' + n' + p' + q' + r' \tag{34a}$$

$$l: \quad 1 = -3a' - b' + c' + d' + f' + g' + l' + 2p' + 3q' + 3r' \tag{34b}$$

$$t: \quad -2 = -b' - c' - f' - 2g' - i' - 2j' - k' - 2l' + m' - 2q' - 2r' \tag{34c}$$

Since only three fundamental units are involved, any three exponents can be expressed in terms of the remaining but indeterminate exponents. Selecting ρ_f, l, and V as the fundamental quantities of concern and solving for the exponents a', d', and f' associated with these physical quantities, the following expressions are obtained from equations (34a), (34b), and (34c), respectively.

$$a' = 1 - b' - n' - p' - q' - r' \tag{35a}$$

$$d' = 1 + 3a' + b' - c' - f' - g' - l' - 2p' - 3q' - 3r' \tag{35b}$$

$$f' = 2 - b' - c' - 2g' - i' - 2j' - k' - 2l' + m' - 2q' - 2r' \tag{35c}$$

Substituting equations (35a) and (35c) for a' and f' in equation (35b),

$$d' = 2 - b' - 3n' - 5p' - 4q' - 4r' + g' + i' + 2j' + k' + l' - m' \tag{35d}$$

By substituting equations (35a), (35d), and (35c) for the exponents a', c', and f', respectively, in equation (32) and collecting the terms with the same exponents, we obtain the following:

$$F = \rho_f V^2 l^2 \left(\frac{\mu}{\rho_f V l}\right)^{b'} \left(\frac{V_s}{V}\right)^{c'} (\alpha')^{e'} \left(\frac{al}{V^2}\right)^{g'} (\delta)^{h'} \left(\frac{\Omega l}{V}\right)^{i'} \left(\frac{\dot{\Omega} l^2}{V^2}\right)^{j'} \left(\frac{\omega l}{V}\right)^{k'} \left(\frac{gl}{V^2}\right)^{l'} \left(\frac{Vt}{l}\right)^{m'} \left(\frac{m}{\rho_f l^3}\right)^{n'} \left(\frac{I}{\rho_f l^5}\right)^{p'} \left(\frac{EI'}{\rho_f V^2 l^4}\right)^{q'} \left(\frac{GJ'}{\rho_f V^2 l^4}\right)^{r'} \tag{36}$$

or

$$\frac{F}{1/2\rho_f V^2 l^2} = f\left(\frac{\rho_f V l}{\mu}, \frac{V}{V_s}, \alpha', \frac{al}{V^2}, \delta, \frac{\Omega l}{V}, \frac{\dot{\Omega} l^2}{V^2}, \frac{\omega l}{V}, \frac{V^2}{lg}, \frac{Vt}{l}, \frac{m}{\rho_f l^3}, \frac{I}{\rho_f l^5}, \frac{EI'}{\rho_f V^2 l^4}, \frac{GJ'}{\rho_f V^2 l^4}\right) \tag{37}$$

which is in the same format as equation (2a). Equation (2b) is obtained similarly.

REFERENCES

1. Bridgman, Percy W.: Dimensional Analysis. AMS Press, Inc., 1976 (reprint of 1931 rev. ed.).

2. Langhaar, Henry L.: Dimensional Analysis and Theory of Models. John Wiley & Sons, Inc., 1951.

3. Mechtly, E. A.: The International System of Units - Physical Constants and Conversion Factors. Second Revision. NASA SP-7012, 1973.

4. Paterson, J. H.; and McBride, E. E.: C-5A Stability, Control and Loads Technology. Paper presented at the Seminar on Elastic Airplane Stability, Control and Response, University of Kansas, Lawrence, Kansas, June 10-14, 1968.

5. Polhamus, Edward C.; Kilgore, Robert A.; Adcock, Jerry B.; and Ray, Edward J.: The Langley Cryogenic High Reynolds Number Wind-Tunnel Program. Astronaut. & Aeronaut., vol. 12, no. 10, Oct. 1974, pp. 30-40.

6. Kilgore, Robert A.; Adcock, Jerry B.; and Ray, Edward J.: Simulation of Flight Test Conditions in the Langley Pilot Transonic Cryogenic Tunnel. NASA TN D-7811, 1974.

7. Dommasch, Daniel O.; Sherby, Sydney S.; and Connolly, Thomas F.: Airplane Aerodynamics. Fourth ed., Pitman Publishing Corp., 1967.

8. Jones, George W., Jr.; Cincotta, Joseph J.; and Walker, Robert W.: Aerodynamic Forces on a Stationary and Oscillating Circular Cylinder at High Reynolds Numbers. NASA TR R-300, 1969.

9. Campbell, John P.; Johnson, Joseph L., Jr.; and Hewes, Donald E.: Low-Speed Study of the Effect of Frequency on the Stability Derivatives of Wings Oscillating in Yaw With Particular Reference to High Angle-of-Attack Conditions. NACA RM L55H05, 1955.

10. Bird, John D.; Jacquet, Byron M.; and Cowan, John W.: Effect of Fuselage and Tail Surfaces on Low-Speed Yawing Characteristics of a Swept-Wing Model as Determined in Curved-Flow Test Section of Langley Stability Tunnel. NACA TN 2483, 1951.

11. Fisher, Lewis R.: Experimental Determination of the Effects of Frequency and Amplitude on the Lateral Stability Derivatives for a Delta, Swept, and an Unswept Wing Oscillating in Yaw. NACA RM L56A19, 1956.

12. Neihouse, Anshal I.; Klinar, Walter J.; and Scher, Stanley H.: Status of Spin Research for Recent Airplane Designs. NASA TR R-57, 1960.

13. Von Doenhoff, Albert E.: Principles of Model Testing. High Speed Aerodynamics and Jet Propulsion, Volume VIII - High Speed Problems of Aircraft and Experimental Methods, Part 2, F. E. Goddard, ed., Princeton Univ. Press, 1961, p. 442.

14. Roskam, J.; Holgate, T.; and Shimizu, G.: Development and Use of Elastic Wind-Tunnel Models in Predicting Longitudinal Stability Derivatives of Elastic Airplanes. AIAA Paper 68-56, Jan. 1968.

15. MacLachlan, Robert; and Letko, William: Correlation of Two Experimental Methods of Determining the Rolling Characteristics of Unswept Wings. NACA TN 1309, 1947.

16. Scherberg, Max; and Rhode, R. V.: Mass Distribution and Performance of Free Flight Models. NACA TN 268, 1927.

17. Zimmerman, C. H.: Preliminary Tests in the N. A. C. A. Free-Spinning Wind Tunnel. NACA Rept. 557, 1936.

18. Chambers, Joseph R.; Anglin, Ernie L.; and Bowman, James S., Jr.: Effects of a Pointed Nose on Spin Characteristics of a Fighter Airplane Model Including Correlation With Theoretical Calculations. NASA TN D-5921, 1970.

19. Bowman, James S., Jr.: Summary of Spin Technology as Related to Light General-Aviation Airplanes. NASA TN D-6575, 1971.

20. Shortal, Joseph A.; and Osterhout, Clayton J.: Preliminary Stability and Control Tests in the NACA Free-Flight Wind Tunnel and Correlation With Full-Scale Flight Tests. NACA TN 810, 1941.

21. Paulson, John W.: Investigation of the Low-Speed Flight Characteristics of a 1/15-Scale Model of the Convair XB-58 Airplane. NACA RM SL57K19, 1957.

22. Libbey, Charles E.; and Burk, Sanger M., Jr.: A Technique Utilizing Free-Flying Radio-Controlled Models To Study the Incipient- and Developed-Spin Characteristics of Airplanes. NASA Memo 2-6-59L, 1959.

23. Lee, Henry A.; and Libbey, Charles E.: Incipient- and Developed-Spin and Recovery Characteristics of a Modern High-Speed Fighter Design With Low Aspect Ratio as Determined From Dynamic-Model Tests. NASA TN D-956, 1961.

24. Chambers, Joseph R.: Status of Model Testing Techniques. Stall/Post-Stall/Spin Symposium, paper J, Air Force Flight Dynamics Lab. (FGC), Wright-Patterson AFB, Ohio, 15-17 Dec. 1971, pp. J-1 to J-25.

25. Gilbert, William P.: Automatic Spin Prevention. Stall/Post-Stall/Spin Symposium, paper S, Air Force Flight Dynamics Lab. (FGC), Wright-Patterson AFB, Ohio, 15-17 Dec. 1971, pp. S-1 to S-12.

26. Edwards, J. W.: Flight-Test Experience in Digital Control of a Remotely Piloted Vehicle. AIAA Paper 72-883, Aug. 1972.

27. Edwards, John W.; and Deets, Dwain A.: Development of a Remote Digital Augmentation System and Application to a Remotely Piloted Research Vehicle. NASA TN D-7941, 1975.

28. Holleman, Euclid C., compiler: Initial Results From Flight Testing a Large, Remotely Piloted Airplane Model. NASA TM X-56024, 1974.

29. Layton, G. P.: NASA Flight Research Center Scale F-15 Remotely Piloted Research Vehicle Program. Advancements in Flight Test Engineering - Proceedings of the Fifth Annual Symposium, Soc. of Flight Test Eng., 1974, pp. 1-63 to 1-76.

30. U.S. Standard Atmosphere, 1962. NASA, U.S. Air Force, U.S. Weather Bur., Dec. 1962.

31. Weber, Ernst: Physical Units and Standards. Handbook of Engineering Fundamentals, Ovid W. Eshbach and Mott Souders, eds., Third ed., John Wiley & Sons, Inc., c. 1975, pp. 385-427.

TABLE 1.—PERTINENT QUANTITIES USED TO ESTABLISH DIMENSIONAL HOMOGENEITY IN FORCE AND MOMENT EQUATIONS

Symbol	Description	Dimension
F	Force	mlt^{-2}
M'	Moment	ml^2t^{-2}
ρ_f	Fluid mass density	ml^{-3}
μ	Coefficient of absolute viscosity	$ml^{-1}t^{-1}$
V_s	Velocity of sound (index of fluid elasticity)	lt^{-1}
l	Characteristic length	l
α'	Attitude of aircraft	— — —
V	Linear velocity	lt^{-1}
a	Linear acceleration	lt^{-2}
δ	Angular displacement (control surface)	— — —
Ω	Angular velocity	t^{-1}
$\dot{\Omega}$	Angular acceleration	t^{-2}
ω	Oscillatory frequency	t^{-1}
g	Acceleration of gravity	lt^{-2}
t	Time	t
m	Mass of aircraft	m
I	Mass moment (or product) of inertia	ml^{-2}
EI'	Bending stiffness	ml^3t^{-2}
GJ'	Torsional stiffness	ml^3t^{-2}

TABLE 2.—SIMILITUDE PARAMETERS AND DEFINITIONS

Parameter	General definition	Applied definition
$\frac{F}{(1/2)\rho_f V^2 l^2}$	Aerodynamic force coefficient (Newton force coefficient)	$C_L, C_D, C_Y, \ldots$
$\frac{M'}{(1/2)\rho_f V^2 l^3}$	Aerodynamic moment coefficient (Newton moment coefficient)	C_m, C_n, C_l
α'	Aircraft attitude (relative to airstream)	α, β
δ	Control surface position	$\delta_e, \delta_a, \delta_r, \ldots$
$\Omega l/V$	Reduced angular velocity	$\frac{q\bar{c}}{2V}, \frac{rb}{2V}, \frac{\dot{\delta}_e\bar{c}}{2V}, \frac{\dot{\delta}_a b}{2V}, \ldots$
$\dot{\Omega} l^2/V^2$	Reduced angular acceleration	$\frac{\dot{q}\bar{c}^2}{4V^2}, \frac{\dot{r}b^2}{4V^2}, \ldots$
al/V^2	Reduced linear acceleration	$\frac{\dot{V}\bar{c}}{2V^2}, \frac{\ddot{z}\bar{c}}{2V^2}, \frac{\dot{w}\bar{c}}{2V^2} \approx \frac{\dot{\alpha}\bar{c}}{2V}, \ldots$
$\omega l/V$	Strouhal number, N_{Str} (reduced oscillatory frequency)	- - - - - - - - - -
$\rho_f V l/\mu$	Reynolds number, N_{Re}	$f\left(\frac{\text{Fluid inertia force}}{\text{Viscous force}}\right)$
V^2/lg	Froude number, N_{Fr}	$f\left(\frac{\text{Inertia force}}{\text{Gravitational force}}\right)$
V/V_s	Mach number, M (fluid compressibility parameter)	$f\left(\frac{\text{Fluid inertia force}}{\text{Fluid pressure force}}\right)$
$m/\rho_f l^3$	Relative density factor	$f(\rho_b/\rho_f), \frac{m}{\rho_f S\bar{c}/2}, \frac{m}{\rho_f Sb/2}$
$I/\rho_f l^5$	Relative mass moment of inertia	- - - - - - - - - -
$EI'/\rho_f V^2 l^4$	Aeroelastic-bending parameter	- - - - - - - - - -
$GJ'/\rho_f V^2 l^4$	Aeroelastic-torsion parameter	- - - - - - - - - -
tV/l	Reduced-time parameter, τ	$\frac{tV}{\bar{c}/2}, \frac{tV}{b/2}$

TABLE 3.- SCALING FACTORS FOR MOUNTED AND RESTRAINED WIND-TUNNEL MODELS

(a) Rigid models. Aerodynamic coefficient = $f(\alpha', \delta, M, N_{Re}, \Omega l/V, N_{Sr}, tV/l)$

Parameter	Ratio	Scaling factor					
		Incompressible flow			Compressible flow		
		Static tests	Dynamic tests: Curved flow or rotating model	Dynamic tests: Oscillating model	Static tests	Dynamic tests: Rotating model	Dynamic tests: Oscillating model
Length	l_m/l_A	n	n	n	n	n	n
Vehicle attitude	α'_m/α'_A	1	1	1	1	1	1
Control surface deflection	δ_m/δ_A	1	1	1	1	1	1
Mach number	M_m/M_A	- - - -	- - - - - - - -	- - - - - - - -	1	1	1
Linear velocity	V_m/V_A	V_m/V_A	V_m/V_A	V_m/V_A	$V_{s_m}M_m/V_{s_A}M_A = R_{V_s}$	R_{V_s}	R_{V_s}
Reynolds number*	$(N_{Re})_m/(N_{Re})_A$	$\left(\frac{\rho_{f_m}V_m}{\mu_m}\Big/\frac{\rho_{f_A}V_A}{\mu_A}\right)n = \left(\frac{\nu_A}{\nu_m}\right)\left(\frac{V_m}{V_A}\right)n = 1$			$\frac{\nu_A}{\nu_m}R_{V_s}n = 1$		
Reduced angular rate	$\left(\frac{\Omega l}{V}\right)_m\Big/\left(\frac{\Omega l}{V}\right)_A$	- - - -	1	1	- - - - - - - - - - - -	1	1
Angular rate	Ω_m/Ω_A	- - - -	$(V_m/V_A)/n$	$(V_m/V_A)/n$	- - - - - - - - - - - -	R_{V_s}/n	R_{V_s}/n
Radius of curvature of flow in curved flow tests	r_m/r_A	- - - -	n	- - - - - - - -	- - - - - - - - - - - -	- - - - -	- - - - - - -
Strouhal number	$\left(\frac{\omega l}{V}\right)_m\Big/\left(\frac{\omega l}{V}\right)_A$	- - - -	- - - - - - - -	1	- - - - - - - - - - - -	- - - - -	1
Oscillatory frequency	ω_m/ω_A	- - - -	- - - - - - - -	$(V_m/V_A)/n$	- - - - - - - - - - - -	- - - - -	R_{V_s}/n
Reduced time	$\left(\frac{tV}{l}\right)_m\Big/\left(\frac{tV}{l}\right)_A$	- - - -	1	1	- - - - - - - - - - - -	1	1
Time	t_m/t_A	- - - -	$(V_A/V_m)n$	$(V_A/V_m)n$	- - - - - - - - - - - -	n/R_{V_s}	n/R_{V_s}
Angular displacement	φ'_m/φ'_A	- - - -	1	1	- - - - - - - - - - - -	1	1

*Normally difficult to scale for similitude; transition grit usually employed on model to approximate Reynolds number similitude.

TABLE 3.—Concluded

(b) Aeroelastic models. Aerodynamic coefficient = $f\left(\alpha', \delta, M, N_{Re}, \frac{m}{\rho_f l^3}, \frac{I}{\rho_f l^5}, \frac{EI'}{\bar{q} l^4}, \frac{GJ'}{\bar{q} l^4}\right)$

Parameter	Ratio	Scaling factor
Length	l_m / l_A	n
Vehicle attitude	α'_m / α'_A	1
Control surface deflection	δ_m / δ_A	1
Mach number	M_m / M_A	1
Linear velocity	V_m / V_A	R_{V_s}
Fluid mass density	ρ_{f_m} / ρ_{f_A}	ρ_{f_m} / ρ_{f_A}
Dynamic pressure	$\bar{q}_m / \bar{q}_A$	$\left(\rho_{f_m} / \rho_{f_A}\right) R_{V_s}^{\ 2}$
Reynolds number*	$(N_{Re})_m / (N_{Re})_A$	$(\nu_A / \nu_m) R_{V_s}\ n = 1$
Relative density factor†	$\left(\frac{m}{\rho_f l^3}\right)_m \Big/ \left(\frac{m}{\rho_f l^3}\right)_A$	1
Mass†	m_m / m_A	$\left(\rho_{f_m} / \rho_{f_A}\right) n^3$
Relative mass moment of inertia†	$\left(\frac{I}{\rho_f l^5}\right)_m \Big/ \left(\frac{I}{\rho_f l^5}\right)_A$	1
Mass moment of inertia†	I_m / I_A	$\left(\rho_{f_m} / \rho_{f_A}\right) n^5$
Aeroelastic bending (slope)	$\left(\frac{EI'}{\bar{q} l^4}\right)_m \Big/ \left(\frac{EI'}{\bar{q} l^4}\right)_A$	1
Bending stiffness	$(EI')_m / (EI')_A$	$(\bar{q}_m / \bar{q}_A) n^4 = \left(\rho_{f_m} / \rho_{f_A}\right) R_{V_s}^{\ 2} n^4$
Area moment of inertia	I'_m / I'_A	$(\bar{q}_m / \bar{q}_A)(E_A / E_m) n^4$
Aeroelastic torsion (angular twist per unit length)	$\left(\frac{GJ'}{\bar{q} l^4}\right)_m \Big/ \left(\frac{GJ'}{\bar{q} l^4}\right)_A$	1
Torsional stiffness	$(GJ')_m / (GJ')_A$	$(\bar{q}_m / \bar{q}_A) n^4 = \left(\rho_{f_m} / \rho_{f_A}\right) R_{V_s}^{\ 2} n^4$
Area torsional moment of inertia	J'_m / J'_A	$(\bar{q}_m / \bar{q}_A)(G_A / G_m) n^4$
Strouhal number	$\left(\frac{\omega l}{V}\right)_m \Big/ \left(\frac{\omega l}{V}\right)_A$	1
Flutter frequency	ω_m / ω_A	R_{V_s} / n

*Similitude normally not attainable; transition grit usually employed to approximate similitude.

†Similitude and scaling requirements usually not satisfied on performance and stability and control models.

TABLE 4.—SCALE FACTORS FOR FREE-FLYING MODELS

$$\left[\text{Aerodynamic coefficient} = f\left(\alpha', \delta, N_{Fr}, M, N_{Re}, \frac{\Omega\ell}{V}, N_{Str}, \frac{tV}{\ell}, \frac{m}{\rho_f \ell^3}, \frac{I}{\rho_f \ell^5}, \frac{EI'}{\rho_f V^2 \ell^4}, \frac{GJ'}{\rho_f V^2 \ell^4}\right)\right]$$

(a) Flow and dynamic scale factors

Parameter	Ratio	Scaling factor	
		Froude scaling	Mach scaling
Length	ℓ_m/ℓ_A	n	n
Vehicle attitude	α'_m/α'_A	1	1*
Control surface deflection	δ_m/δ_A	1	1
Froude number	$\left(\frac{V^2}{\ell g}\right)_m \Big/ \left(\frac{V^2}{\ell g}\right)_A$	1	$\left(\frac{g_A}{g_m}\right) R_{V_s}{}^2 (1/n) = 1$
Gravity field	g_m/g_A	1	$R_{V_s}{}^2 (1/n)$
Velocity	V_m/V_A	$n^{1/2}$	R_{V_s}
Mach number	M_m/M_A	$n^{1/2}/R_{V_s}$	1
Fluid density	ρ_{f_m}/ρ_{f_A}	ρ_{f_m}/ρ_{f_A}	ρ_{f_m}/ρ_{f_A}
Dynamic pressure	$\bar{q}_m/\bar{q}_A$	$\left(\rho_{f_m}/\rho_{f_A}\right) n$	$\left(\rho_{f_m}/\rho_{f_A}\right) R_{V_s}{}^2$
Reynolds number	$\left(N_{Re}\right)_m \Big/ \left(N_{Re}\right)_A$	$(\nu_A/\nu_m) n^{3/2}$	$(\nu_A/\nu_m) R_{V_s} n$
Reduced angular rate	$\left(\frac{\Omega\ell}{V}\right)_m \Big/ \left(\frac{\Omega\ell}{V}\right)_A$	1	1
Angular rate	Ω_m/Ω_A	$n^{-1/2}$	R_{V_s}/n
Reduced time	$\left(\frac{tV}{\ell}\right)_m \Big/ \left(\frac{tV}{\ell}\right)_A$	1	1
Time	t_m/t_A	$n^{1/2}$	n/R_{V_s}
Angular displacement	φ'_m/φ'_A	1	1
Angular acceleration	$\dot{\Omega}_m/\dot{\Omega}_A$	n^{-1}	$R_{V_s}{}^2/n^2$
Linear displacement	s_m/s_A	n	n
Linear acceleration	a_m/a_A	1	$R_{V_s}{}^2/n$
Strouhal number	$\left(\frac{\omega\ell}{V}\right)_m \Big/ \left(\frac{\omega\ell}{V}\right)_A$	1	1
Oscillatory frequency	ω_m/ω_A	$n^{-1/2}$	R_{V_s}/n

*In Mach scaling, ability to satisfy attitude scaling is dependent on satisfying Froude number similitude.

TABLE 4.—Concluded

(b) Mass, moment of inertia, and aeroelastic scale factors

Parameter	Ratio	Scaling factor		
		Rigid model, Froude and Mach scaling	Flexible model	
			Froude scaling	Mach scaling
Length	ℓ_m/ℓ_A	n	n	n
Relative density factor	$\left(\frac{m}{\rho_f \ell^3}\right)_m \Big/ \left(\frac{m}{\rho_f \ell^3}\right)_A$	1	1	1
Mass	m_m/m_A	$\left(\rho_{f_m}/\rho_{f_A}\right) n^3$	$\left(\rho_{f_m}/\rho_{f_A}\right) n^3$	$\left(\rho_{f_m}/\rho_{f_A}\right) n^3$
Relative mass moment of inertia	$\left(\frac{I}{\rho_f \ell^5}\right)_m \Big/ \left(\frac{I}{\rho_f \ell^5}\right)_A$	1	1	1
Mass moment of inertia	I_m/I_A	$\left(\rho_{f_m}/\rho_{f_A}\right) n^5$	$\left(\rho_{f_m}/\rho_{f_A}\right) n^5$	$\left(\rho_{f_m}/\rho_{f_A}\right) n^5$
Radius of gyration	k_m/k_A	n	n	n
Aeroelastic bending (slope)	$\left(\frac{EI'}{\rho_f V^2 \ell^4}\right)_m \Big/ \left(\frac{EI'}{\rho_f V^2 \ell^4}\right)_A$	----------	1	1
Bending stiffness	$(EI')_m/(EI')_A$	--------	$(\bar{q}_m/\bar{q}_A)n^4 = \left(\rho_{f_m}/\rho_{f_A}\right) n^5$	$(\bar{q}_m/\bar{q}_A)n^4 = \left(\rho_{f_m}/\rho_{f_A}\right) R_{V_s}{}^2 n^4$
Area moment of inertia	I'_m/I'_A	--------	$(\bar{q}_m/\bar{q}_A)\left(\frac{E_A}{E_m}\right)n^4 = \left(\rho_{f_m}/\rho_{f_A}\right)\left(\frac{E_A}{E_m}\right)n^5$	$(\bar{q}_m/\bar{q}_A)\left(\frac{E_A}{E_m}\right)n^4 = \left(\rho_{f_m}/\rho_{f_A}\right)\left(\frac{E_A}{E_m}\right)R_{V_s}{}^2 n^4$
Aeroelastic torsion	$\left(\frac{GJ'}{\rho_f V^2 \ell^4}\right)_m \Big/ \left(\frac{GJ'}{\rho_f V^2 \ell^4}\right)_A$	--------	1	1
Torsional stiffness	$(GJ')_m/(GJ')_A$	----------	$(\bar{q}_m/\bar{q}_A)n^4 = \left(\rho_{f_m}/\rho_{f_A}\right) n^5$	$(\bar{q}_m/\bar{q}_A)n^4 = \left(\rho_{f_m}/\rho_{f_A}\right) R_{V_s}{}^2 n^4$
Area torsional moment of inertia	J'_m/J'_A	--------	$(\bar{q}_m/\bar{q}_A)\left(\frac{G_A}{G_m}\right)n^4 = \left(\rho_{f_m}/\rho_{f_A}\right)\left(\frac{G_A}{G_m}\right)n^5$	$(\bar{q}_m/\bar{q}_A)\left(\frac{G_A}{G_m}\right)n^4 = \left(\rho_{f_m}/\rho_{f_A}\right)\left(\frac{G_A}{G_m}\right)R_{V_s}{}^2 n^4$

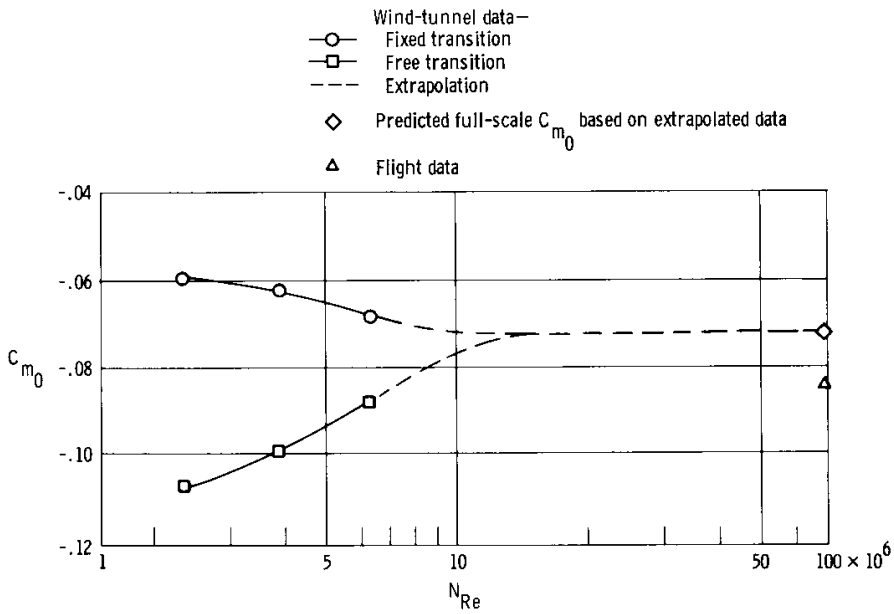

Figure 1. Effect of Reynolds number on wing-body zero-lift pitching moment. M = 0.825; C-141 airplane (ref. 4).

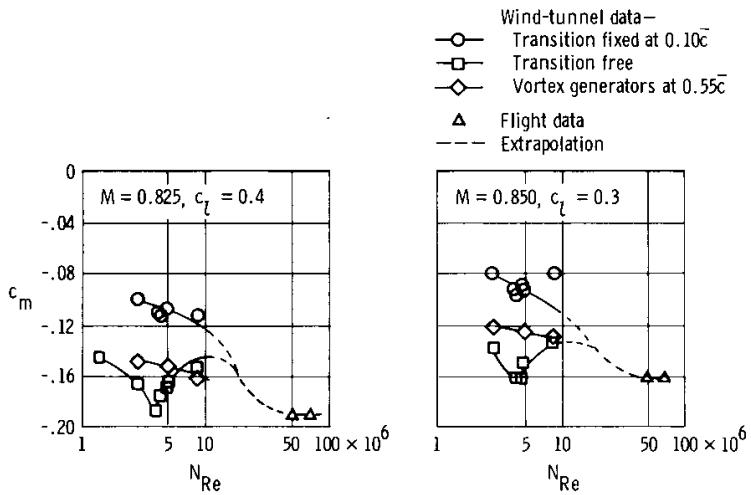

(a) Spanwise station 0.637 (b/2).

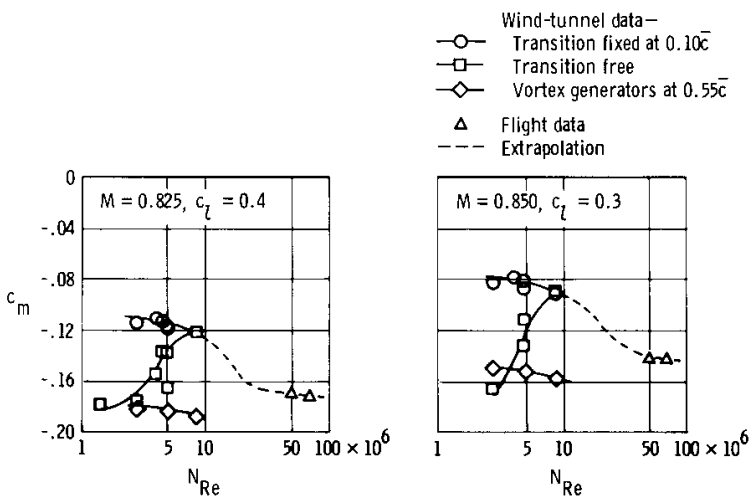

(b) Spanwise station 0.389 (b/2).

Figure 2. Scale effects on wing-section pitching moment coefficient of C-141 airplane (ref. 4).

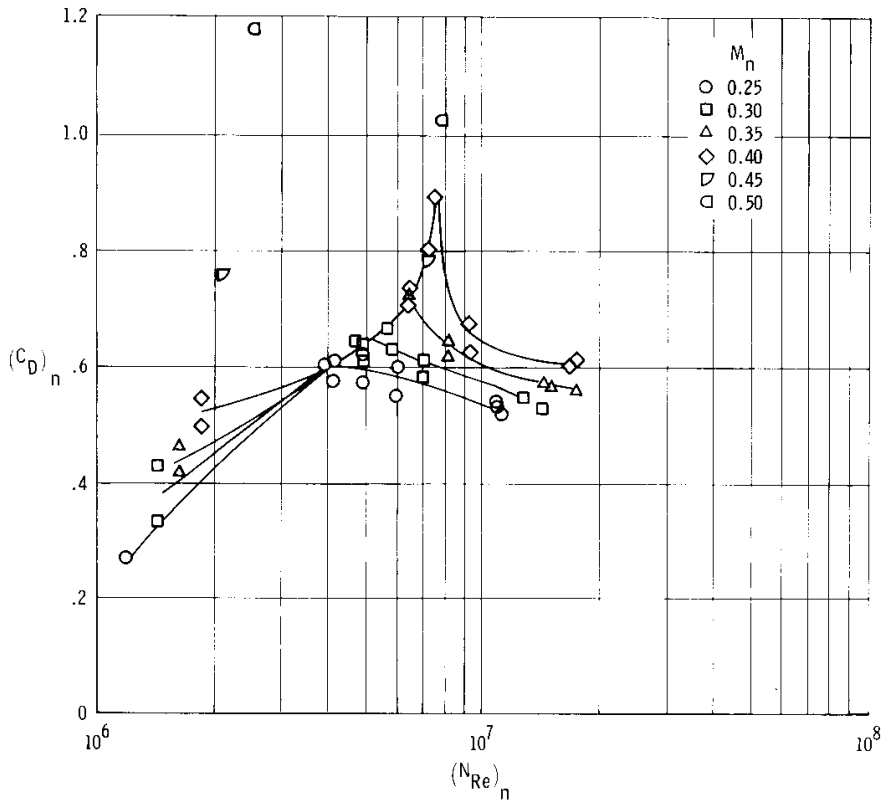

Figure 3. Variation of crossflow drag coefficient with crossflow Reynolds number for circular cylinders at supercritical Reynolds numbers and crossflow Mach numbers from 0.25 to 0.50 (ref. 8).

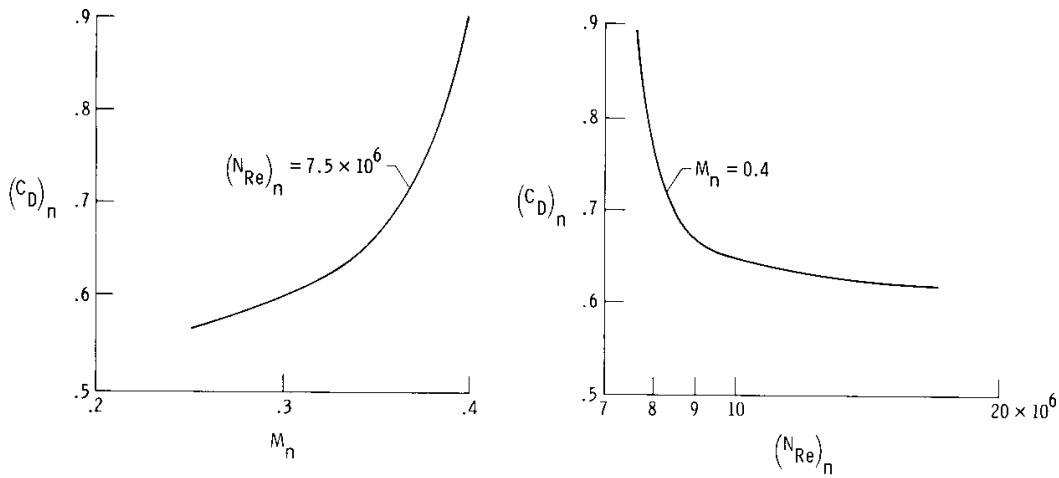

(a) Drag increase due to Mach number.

(b) Drag decrease due to Reynolds number.

Figure 4. Peak in crossflow drag coefficient of cylinder as combined effect of crossflow Mach number and Reynolds number (ref. 8).

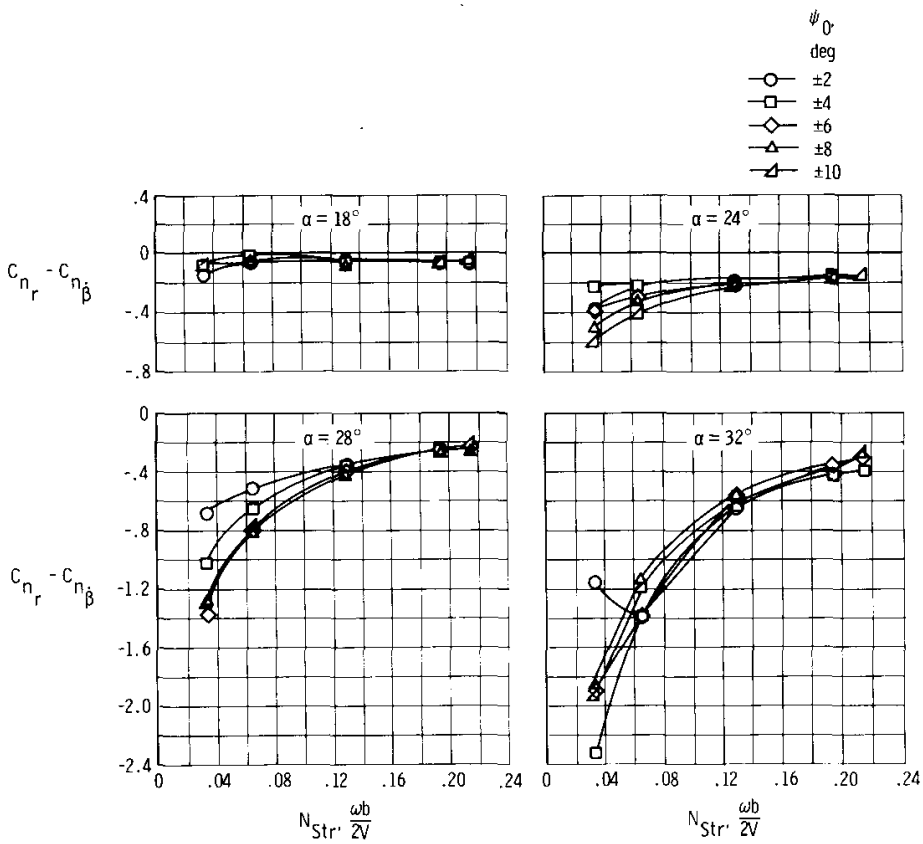

(a) $C_{n_r} - C_{n_{\dot\beta}}$.

Figure 5. Variation of lateral-directional stability derivatives of a delta wing with Strouhal number and amplitude of oscillation (ref. 11).

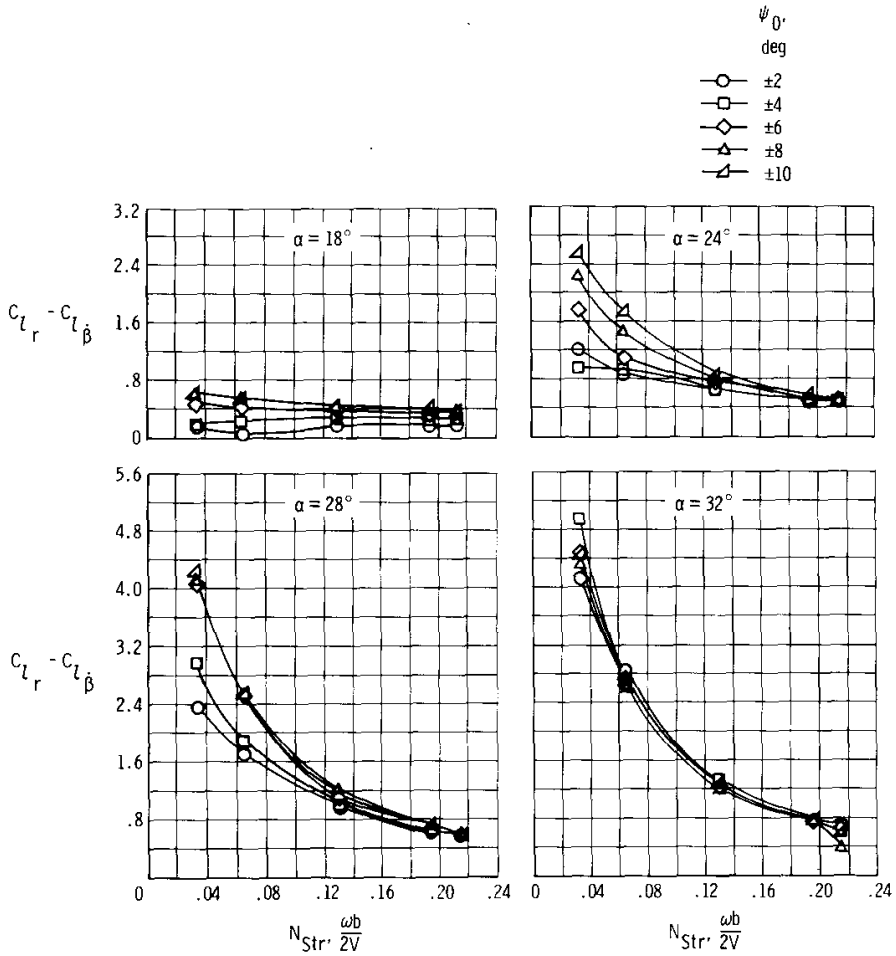

(b) $C_{l_r} - C_{l_{\dot\beta}}$.

Figure 5. Continued.

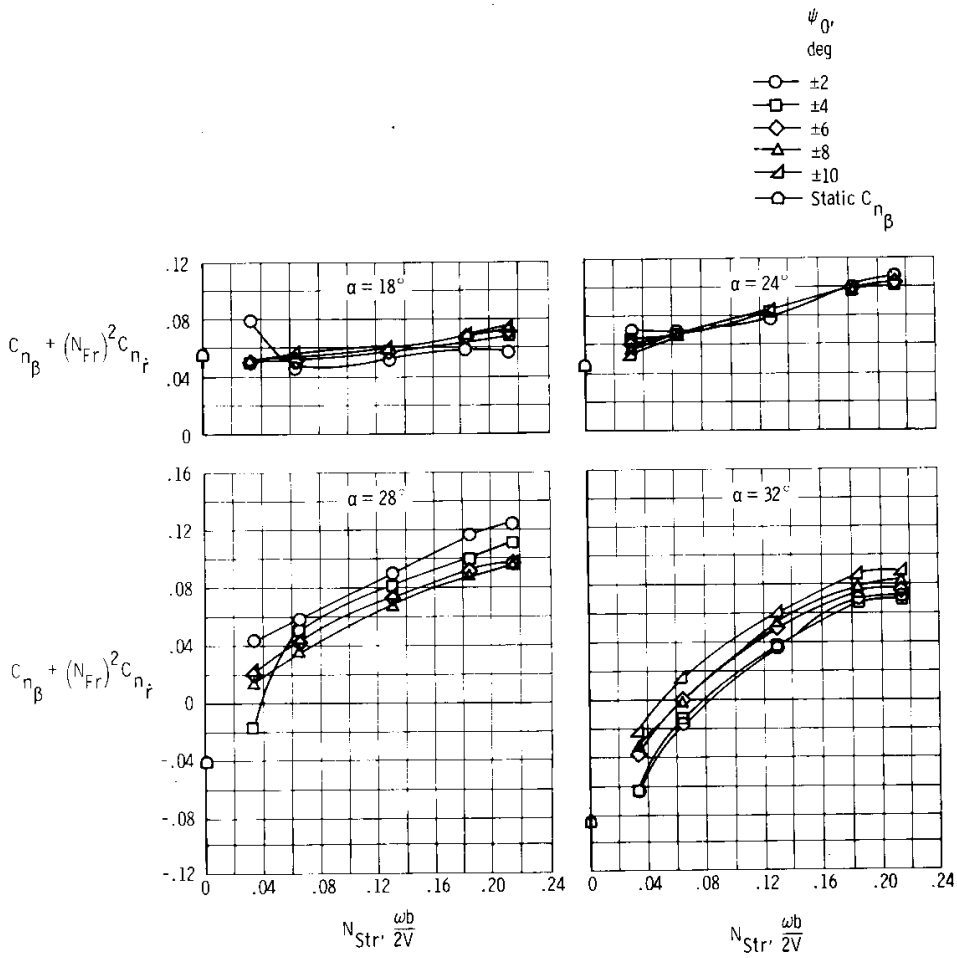

(c) $C_{n_\beta} + (N_{Fr})^2 C_{n_{\dot{r}}}$.

Figure 5. Continued.

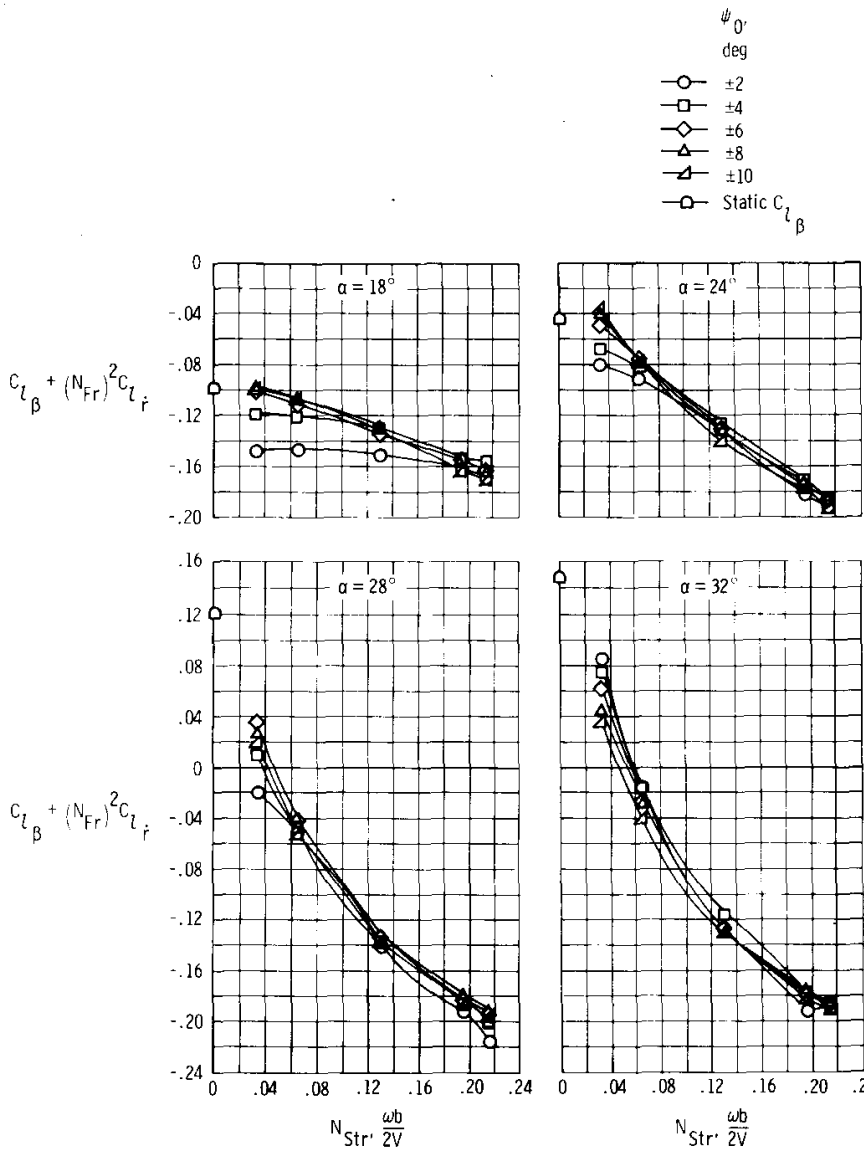

(d) $C_{l_\beta} + (N_{Fr})^2 C_{l_{\dot{r}}}$.

Figure 5. Concluded.

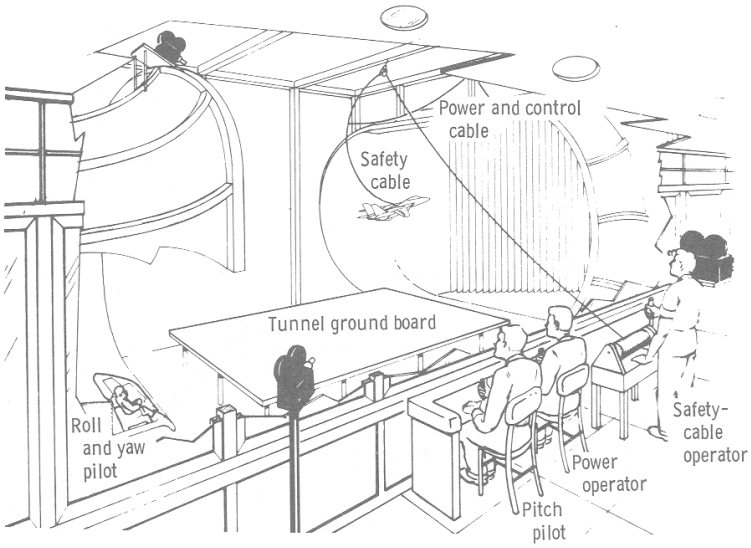

Figure 6. Test setup for wind-tunnel free-flight tests.

Figure 7. Drop model mounted on helicopter launch rig.

Figure 8. Ground control unit for drop-model tests.

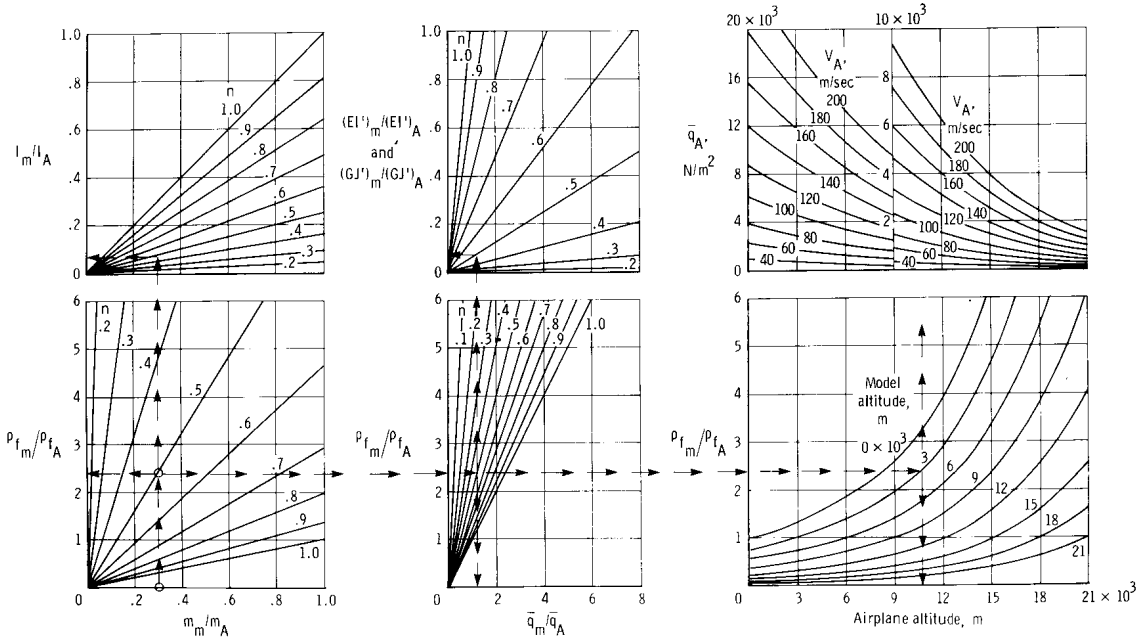

(a) International System of Units.

Figure 9. Froude-scaled model-to-airplane ratios of mass, moments of inertia, and bending and torsional stiffness as functions of model geometric scale, model test altitude, and airplane altitude in atmospheric free-flight model tests.

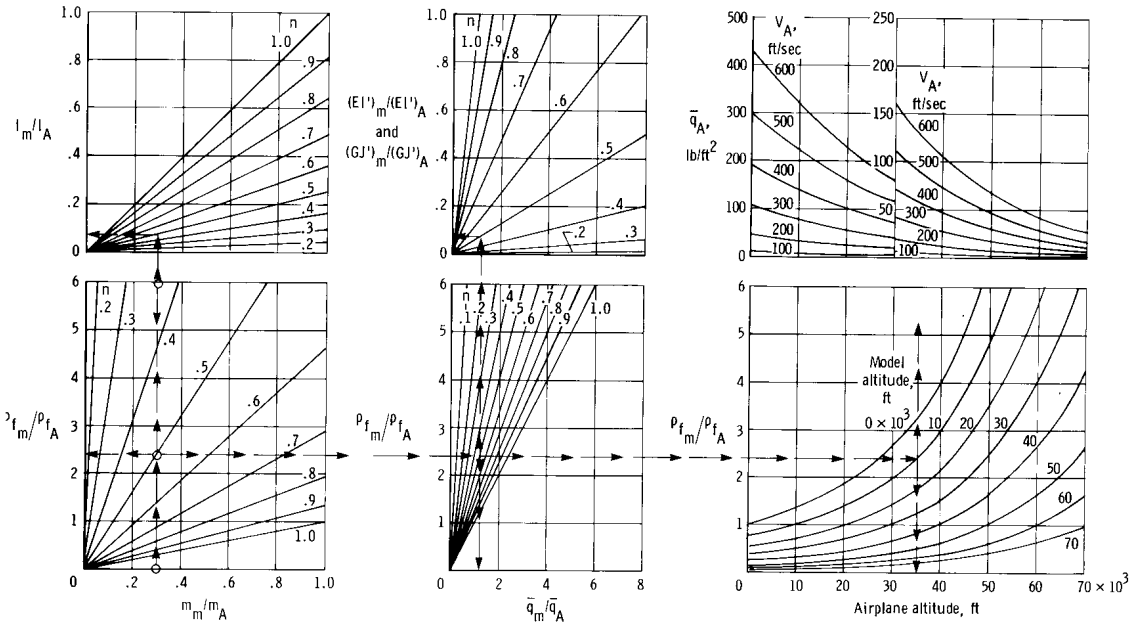

(b) U.S. Customary System of Units.

Figure 9. Concluded.

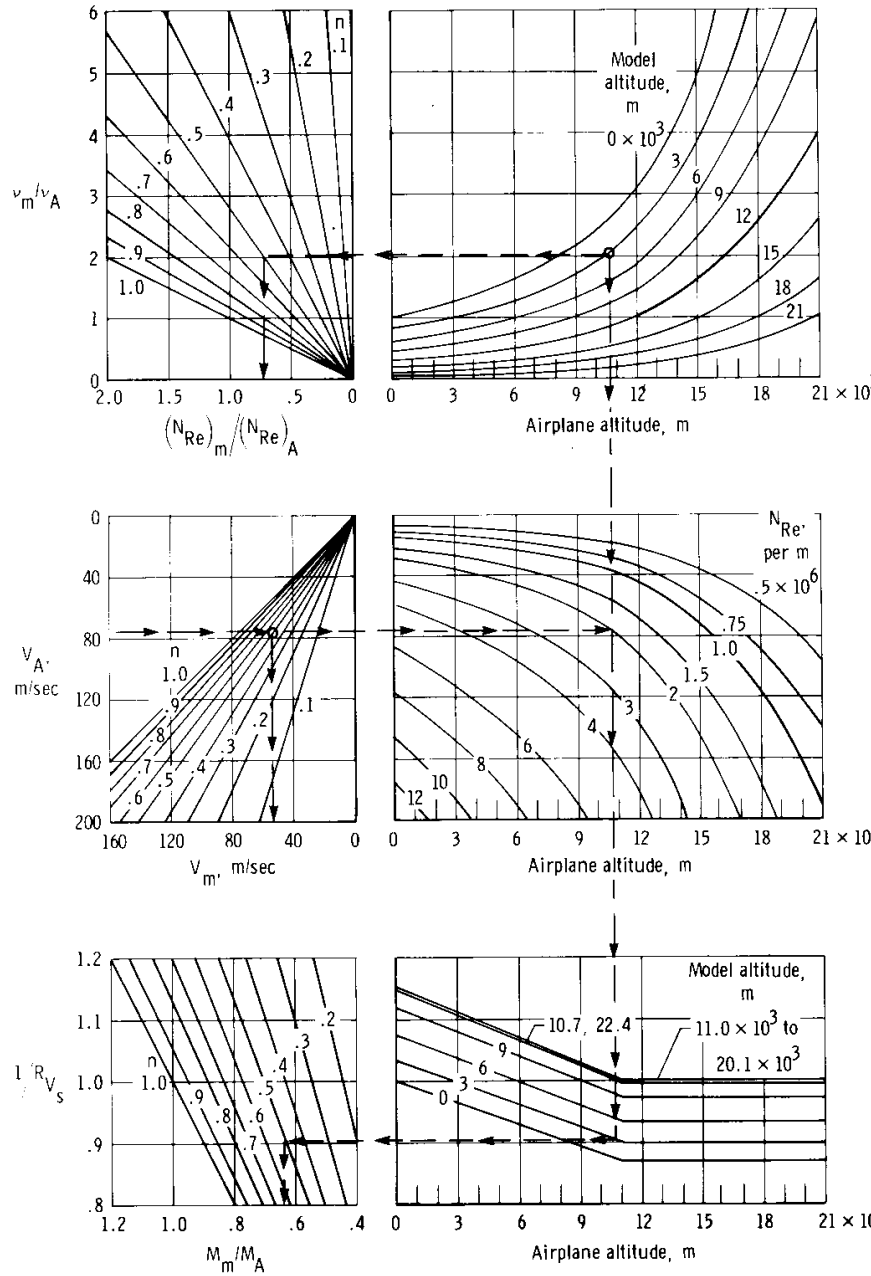

(a) International System of Units.

Figure 10. Froude-scaled model-to-airplane ratios of Reynolds and Mach numbers as functions of model geometric scale, model test altitude, and airplane altitude in atmospheric free-flight model tests.

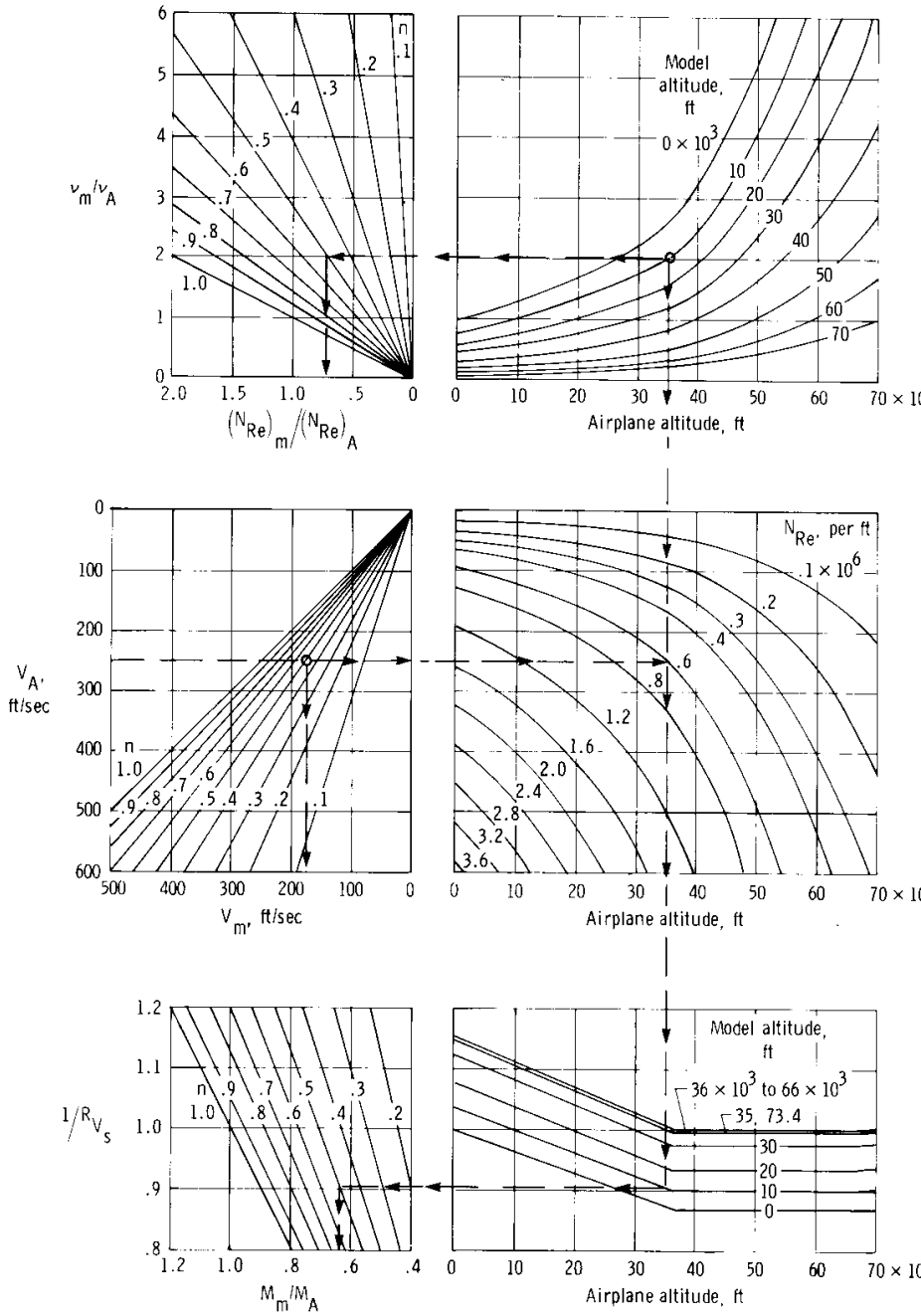

(b) U.S. Customary System of Units.

Figure 10. Concluded.

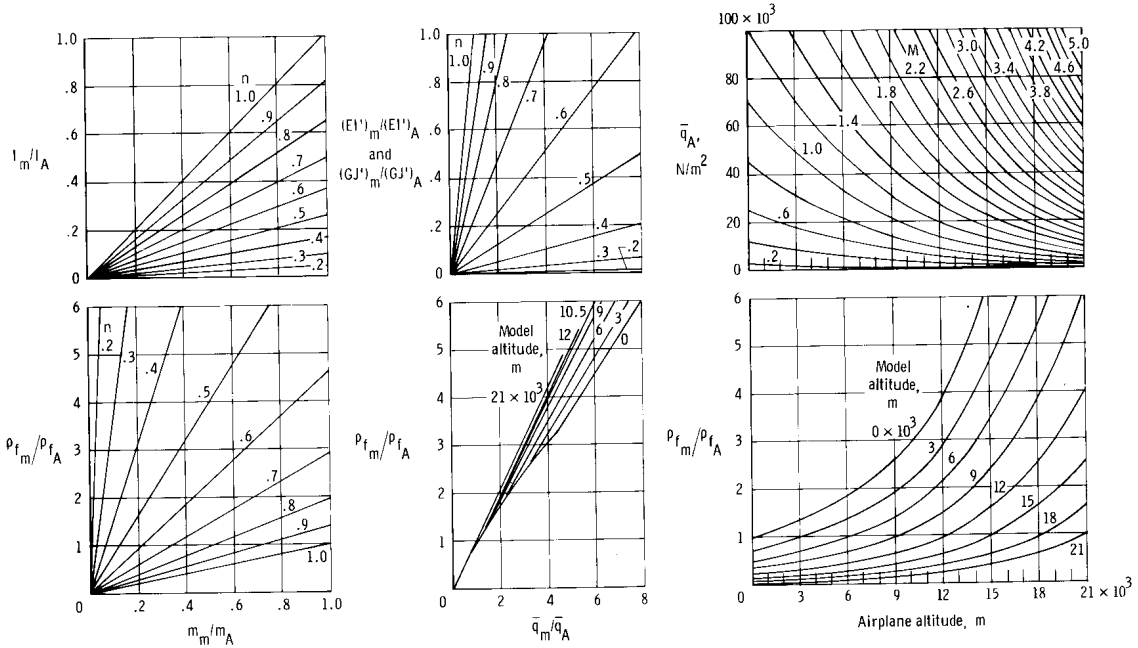

(a) International System of Units.

Figure 11. Mach-scaled model-to-airplane ratios of mass, moments of inertia, and bending and torsional stiffness as functions of model geometric scale, model test altitude, and airplane altitude in atmospheric free-flight model tests.

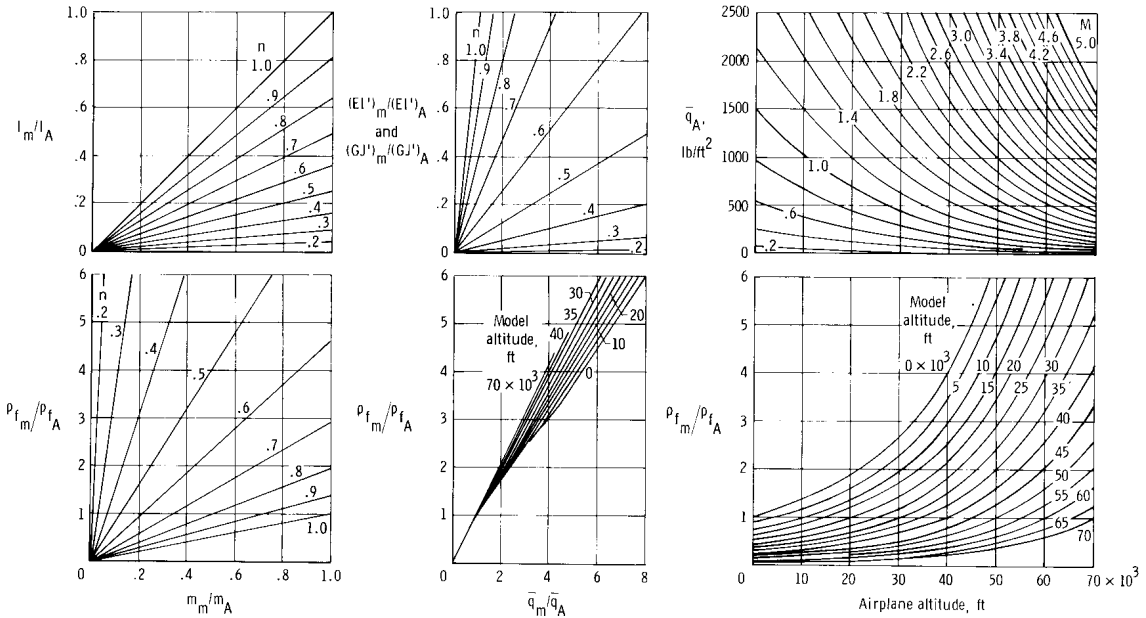

(b) U.S. Customary System of Units.

Figure 11. Concluded.

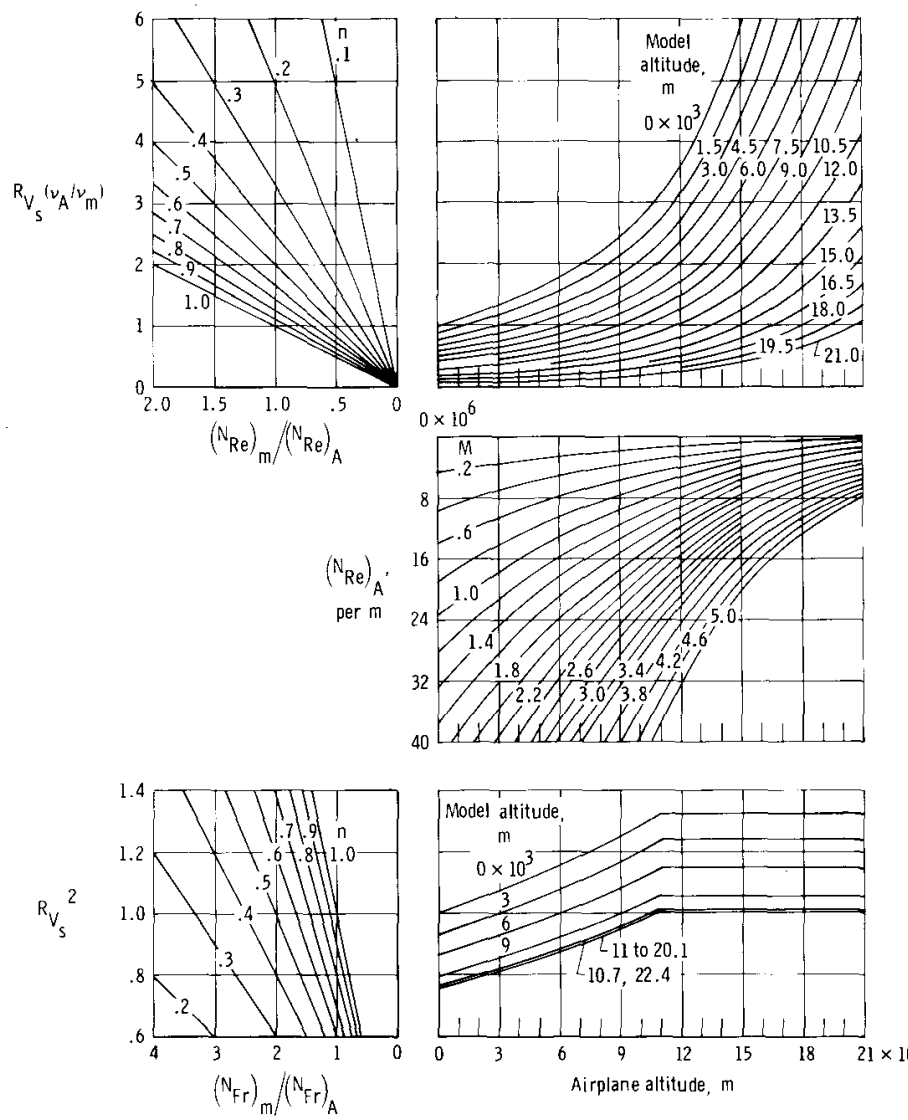

(a) International System of Units.

Figure 12. Mach-scaled model-to-airplane ratios of Reynolds and Froude numbers as functions of model geometric scale, model test altitude, and airplane altitude in atmospheric free-flight model tests.

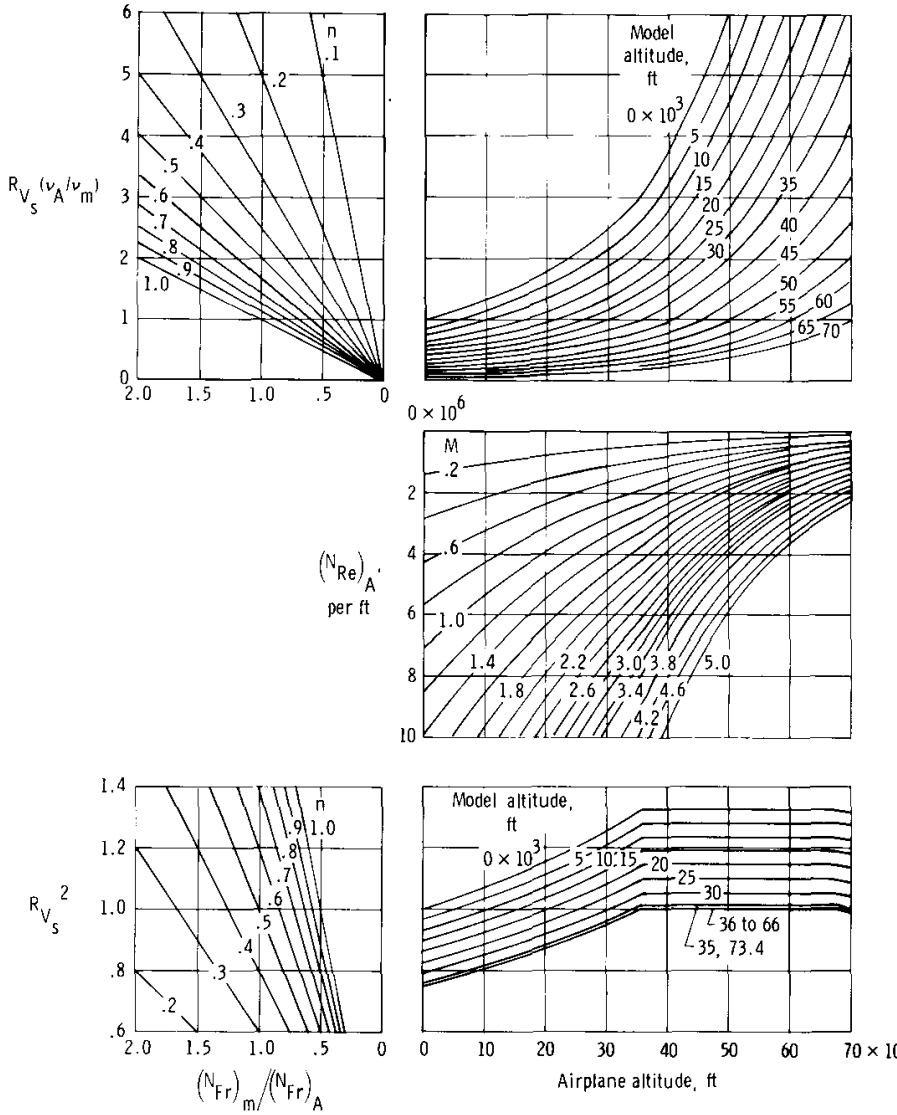

(b) U.S. Customary System of Units.

Figure 12. Concluded.

1. Report No.	2. Government Accession No.	3. Recipient's Catalog No.
NASA TP-1435		

4. Title and Subtitle	5. Report Date
SIMILITUDE REQUIREMENTS AND SCALING RELATIONSHIPS AS APPLIED TO MODEL TESTING	August 1979
	6. Performing Organization Code H-1022
7. Author(s) Chester H. Wolowicz, James S. Bowman, Jr., and William P. Gilbert	8. Performing Organization Report No.
	10. Work Unit No. 505-06-34
9. Performing Organization Name and Address NASA Dryden Flight Research Center P.O. Box 273 Edwards, California 93523	11. Contract or Grant No.
	13. Type of Report and Period Covered Technical Paper
12. Sponsoring Agency Name and Address National Aeronautics and Space Administration Washington, D.C. 20546	14. Sponsoring Agency Code

15. Supplementary Notes

16. Abstract

In general, the available literature presents only the limited aspects of similitude requirements and scaling relationships pertinent to each reported investigation. There is a need, however, for a comprehensive review of the advantages and limitations of wind-tunnel and free-flight model testing techniques with regard to similitude requirements, test objectives, and comparison of model and full-scale results.

This report reviews the similitude requirements for the most general test conditions. These similitude requirements are then considered in relation to the scaling relationships, test technique, test conditions (including supersonic flow), and test objectives. Particular emphasis is placed on satisfying the various similitude requirements for incompressible and compressible flow conditions. For free-flying model tests, the test velocities for incompressible flow are scaled from Froude number similitude requirements and those for compressible flow are scaled from Mach number similitude requirements. Finally, the limitations of various test techniques are indicated, with emphasis on the free-flying model.

17. Key Words (Suggested by Author(s))	18. Distribution Statement
Similitude Scaling Flight tests Model tests	Unclassified-Unlimited STAR category: 05

19. Security Classif. (of this report)	20. Security Classif. (of this page)	21. No. of Pages	22. Price*
Unclassified	Unclassified	65	$4.25

For sale by the National Technical Information Service, Springfield, Virginia 22161

NASA-Langley, 1979